RSC Advances

PAPER

View Article Online
View Journal | View Issue

Cite this: *RSC Adv.*, 2025, **15**, 38846

Zinc-integrated PLGA/chitosan nanofiber mesh: a platform for wound healing applications

Dekonti Davies,[ab] Alexis Moody,[c] Sita Shrestha,[b] Reedwan Bin Zafar Auniq,[d] Kiran Subedi,[e] Jagannathan Sankar[a] and Narayan Bhattarai *[bc]

Non-healing wounds present significant challenges to patients and healthcare systems, often causing infections and chronic pain due to impaired self-regeneration. Zinc (Zn) shows promise in biomedical applications, particularly wound healing, as its degradation releases Zn^{2+} ions that enhance cell proliferation, angiogenesis, and antimicrobial activity. These properties make Zn ideal for bioresorbable wound dressings, scaffolds, and tissue repair coatings. This study aimed to incorporate metallic Zn particles into electrospun nanofiber meshes of poly(D,L-lactic-*co*-glycolic acid) (PLGA) and PLGA/chitosan (PLGA–CH) and evaluate their wound healing potential. We electrospun polymer–Zn nanoparticle mixtures to fabricate composite fibrous meshes. We assessed Zn's impact on scaffolds' physical, chemical, and biological properties, including fiber morphology, chemical composition, mechanical strength, and Zn^{2+} release. Results showed Zn influences PLGA's physical properties without altering chemical composition. Zn-containing meshes released Zn^{2+} ions in a dose-dependent manner. Biological evaluations using 3T3 fibroblasts over three days revealed fiber composition-dependent cytotoxicity, with certain compositions supporting cell proliferation, suggesting potential for tissue remodelling. Given PLGA and chitosan's biocompatibility and biodegradability, incorporating Zn into composite nanofiber meshes presents a promising approach for wound healing and tissue engineering applications.

Received 23rd May 2025
Accepted 26th September 2025

DOI: 10.1039/d5ra03639a

rsc.li/rsc-advances

Introduction

Non-healing wounds significantly burden healthcare systems, affecting approximately 76 million people globally, owing to complications from diabetes, obesity, and cardiovascular diseases. These wounds lose the self-regeneration ability of the skin, causing a risk of severe damage and bacterial infection. While traditional dressings have limitations, like limited porosity, electrospun nanofibers offer promising solutions for tissue regeneration.[1–3]

Electrospun nanofibrous membranes provide high porosity, specific surface area, and customizability. They resemble the physical structure of the extracellular matrix (ECM) and aid in various aspects of wound healing.[4–6] They can be used as sutures, dermal substitutes, and dressings in various wound types.[7]

Ideal wound-healing devices should be absorbable with excellent mechanical properties and safe degradation rates. Biomaterials used for wound healing include metals, ceramics, and polymers. Synthetic polymers offer mechanical strength and degradability but lack cell-binding sites. Natural polymers chemically resemble ECM and have excellent biocompatibility, but face fabrication challenges. Copolymers exhibit a balance of mechanical properties and bio-functionality.[5,6,8]

Poly(D,L-lactic-co-glycolic acid) (PLGA) is a reabsorbable polyester that is ideal for tissue engineering because of its biodegradability and biocompatibility.[9–11] PLGA accelerates angiogenesis and wound healing, but has poor cell affinity and hydrophilicity.[5,12–15] Chitosan (CH), derived from chitin, is used in biomedical applications owing to its biocompatibility, safety, anti-inflammatory and antibacterial properties. It enhances wound healing by promoting collagen migration and fibroblast deposition.[13,14,16,17] CH can enhance degradation rates and serves as an excellent carrier for different wound-healing agents, protecting from side reactions in the wound that may cause deactivation while simultaneously improving their absorption at the target site.[13,16] Additionally, CH is inherently hydrophilic, a crucial property that helps maintain a moist wound environment. This hydrophilicity improves the

[a]*Department of Mechanical Engineering, North Carolina A & T State University, Greensboro, NC, 27411, USA*
[b]*Department of Chemical, Biological, and Bioengineering, North Carolina A & T State University, Greensboro, NC, 27411, USA. E-mail: nbhattar@ncat.edu*
[c]*Department of Applied Science and Technology, North Carolina A & T State University, Greensboro, NC, 27411, USA*
[d]*The Joint School of Nanoscience and Nanoengineering, North Carolina A & T State University, Greensboro, NC, 27411, USA*
[e]*College of Agriculture and Environmental Sciences, North Carolina A&T State University, Greensboro, NC 27411, USA*

wettability of a composite material and facilitates cellular adhesion and proliferation.[18–20]

Polymer nanofiber meshes can be modified with metals like zinc (Zn) for enhanced properties. Zn, as a bioabsorbable metal, offers excellent strength and ductility for load-bearing applications and plays a role in human physiological functions.[21–24] Zn is an essential trace element in the body and has shown promise in other biomedical applications, particularly for bioresorbable wound dressings, scaffolds, and tissue repair coatings, as its degradation releases Zn^{2+} that enhances cell proliferation, angiogenesis, and antimicrobial activity. Zn^{2+} is crucial in wound healing and is involved in various stages from hemostasis to ECM remodelling.[21,25,26] Specifically for cell membrane repair, immune function, and proliferation, Zn is a critical cofactor for many metalloenzymes that are essential for wound healing.[27] Zn has antimicrobial properties and aids in cellular processes, fibroblast differentiation, and tissue recovery. However, excessive Zn intake can lead to toxicity. The U.S. Food and Drug Administration has set the upper intake level of Zn at 40 mg per day.[22,23,28–32]

While previous studies have explored Zn-based scaffolds for wound healing, several key research gaps are addressed in this study. Firstly, few studies have incorporated elemental Zn particles directly into polymer nanofiber meshes. Many studies in the literature are on incorporating zinc oxide into wound dressings. Molaee *et al.*, developed a novel wound dressing incorporating bacterial cellulose with zinc oxide.[33] Kuddushi *et al.* developed composite dressings incorporating sodium alginate and zinc oxide.[34] Nemati *et al.* evaluated zinc oxide and curcumin-loaded electrospun nanofibers for wound healing.[35] Zhou *et al.* fabricated Polycaprolactone (PCL) and chitosan and zinc oxide nanofiber meshes.[29,36] Additionally, the combined use of PLGA, chitosan, and Zn in a single system has not been studied extensively. This study provides insight into the synergistic effects of these materials.

This research aimed to fabricate PLGA and PLGA/chitosan nanofiber meshes with elemental Zn particles and study the impact of Zn on physical, chemical, and biological properties *in vitro*. The methodology for incorporating Zn particles into polymer scaffold nanofiber meshes under inert conditions and their analysis will be based on the approach outlined in previously published research on elemental Mg and Zn.[22,37] We hypothesized that embedded Zn particles in PLGA and PLGA/CH nanofiber mesh scaffolds would yield a more controllable degradation profile to promote wound healing processes. This research focused on fabricating these composite nanofiber meshes, characterizing their physical and chemical properties, and assessing their biological performance *in vitro* (Scheme 1). Through comprehensive analysis of fiber morphology, mechanical strength, zinc release profiles, and cellular interactions, this work provides important insights into the potential of zinc-integrated nanofiber meshes as advanced wound dressing materials. These findings demonstrate the feasibility of tuning the zinc content and polymer composition to optimize scaffold properties for wound healing applications, laying the groundwork for future *in vivo* studies to further evaluate their therapeutic efficacy.

Materials & methods

Materials

Zinc nanoparticles (Zn NPs) (40–60 nm) were purchased from Millipore Sigma (St. Louis, MO, USA). PLGA Resomer ® RG 755 S was purchased from Evonik Corporation (Piscataway, NJ, USA). Chitosan oligomer (MW 7.5k) was purchased from Creative PEG Works (Chapel Hill, NC, USA). Hexafluoro-2-propanol (HFIP) was purchased from Oakwood Chemicals (Estill, SC, USA). Biocompatible silicone-based elastomeric glue (Kwik-Sil™) was obtained from World Precision Instruments (Sarasota, FL, USA). Dulbecco's phosphate-buffered saline (DPBS) and Dulbecco's modified Eagle's medium (DMEM) were obtained from Life

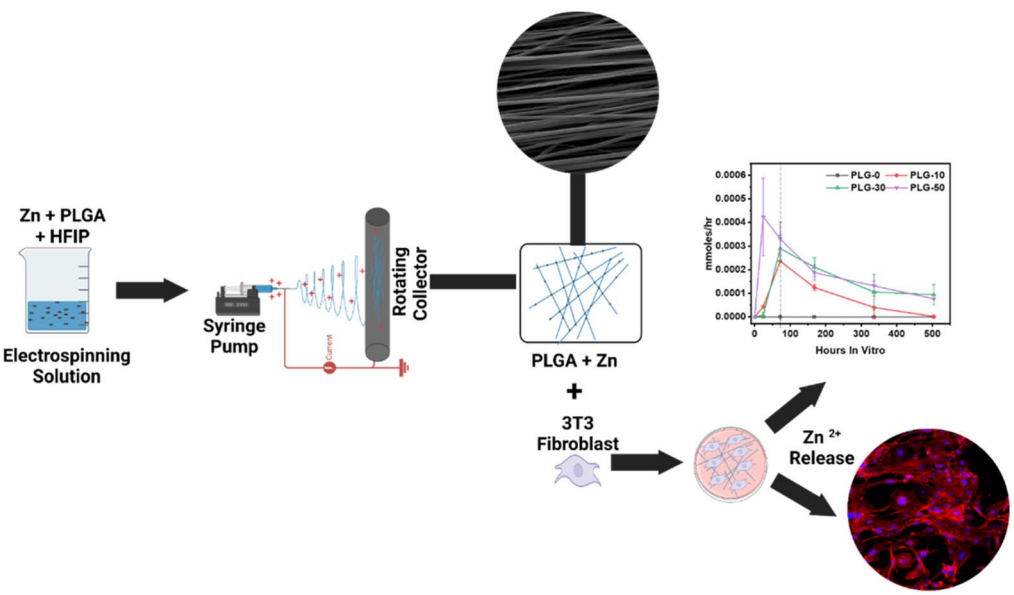

Scheme 1 Schematic illustration of the production of PLGA–Zn and PLGA/CH–Zn nanofiber meshes.

Technologies (Grand Island, NY, USA). The Alamar Blue and lactate dehydrogenase (LDH) assay kits were purchased from Thermo Fisher Scientific (Waltham, MA, USA).

Preparation of PLGA–Zn and PLGA/CH–Zn solutions

PLGA solutions were prepared at 14.5% (w/v) and CH was added to the respective solutions and mixed with HFIP. PLGA–Zn solutions were prepared with different concentrations of the Zn nanopowder. PLGA was added to HFIP and mixed with varying concentrations of Zn (*i.e.*, PLG-0, PLG-1, PLG-3, PLG-5, PLG-10, PLG-30, and PLG-50); numbers 0, 10, 30, and 50 represent the percentage of Zn that was mixed with the PLGA solution. Additionally, five different solutions were initially prepared by incorporating CH and Zn into the already made PLGA solution; these solutions are identified as PLC-0, PLC-1, PLC-3, PLC-5, PLC-10, PLC-30, and PLC-50 (C identifies that chitosan is present in the nanofiber meshes). The initial concentrations of PLGA were mixed at 14.5% w/v and CH was mixed into the solution so that the ratio of PLGA to CH was 80 : 20. The solutions were magnetically stirred for 24 h. Zn nanoparticles were dispersed in the electrospinning solution using a Branson 2510 ultrasonic bath (40 Hz) for 30 minutes to improve dispersion stability. The solution was immediately electrospun after the ultrasonic bath. No additional surfactants were used. The sonicated solution was then immediately loaded into the electrospinning setup. The nanofiber mesh compositions for the PLG and PLC solutions are listed in Tables 1 and 2, respectively.

Fabrication of PLG–Zn and PLC–Zn nanofiber meshes

The electrospinning setup was adapted from previous nanofiber mesh fabrication experiments.[22,37] Briefly, a syringe pump (Model 78-01001, Fisher Scientific, Pittsburgh, PA, USA), high-voltage power supply (Model CZE100PN30, Spellman High Voltage Electronics Corporation, Hauppauge, NY, USA), and metallic collector drum were used to set up the experiment. Approximately 9 mL of the solution was placed in a 10 mL syringe with an attached 18 gauge-diameter hypodermic needle. The flow rate was set to 1.0 mL h^{-1}, the tip of the syringe was placed approximately 12 cm away from the collector, and 15 kV was applied to the solution. The grounded rotating drum of the collector was wrapped with aluminium foil to collect the fibers. The fibers were allowed to dry overnight and were later detached from the foil for physical, chemical, and biological characterization.

Surface morphology analysis

The surface morphologies of the prepared PLG and PLC nanofibers were analyzed using a scanning electron microscope (SEM, Zeiss Auriga series, Oberkochen, Germany) equipped with energy-dispersive X-ray spectroscopy (EDS) (Quantax 70, Bruker Corporation, Billerica, MA, USA). The morphology of the as received-Zn was analyzed in literature.[22] Samples of the PLG and PLC nanofibers were attached to copper tape and sputter-coated with gold–palladium using a coating system (Leica EM ACE200, IL, USA) for 30 s (coating depth = 5 nm) at 15 mA. The SEM images were obtained at an accelerating voltage of 3 kV. SEM images were analyzed for the size distribution of the fibers using the ImageJ 1.54g software (National Institutes of Health, Bethesda, MD, USA). The diameters were converted into pixels using a scale bar. Fifty individual fiber diameters, measured in pixels, were counted from three different SEM images, totalling 150. Data converted from the ImageJ software were used to calculate the average size and standard deviation.

Table 1 Composition of PLGA and Zn in the fabrication of PLG nanofiber meshes

Nanofiber mesh	PLGA : HFIP (w/v%)	PLGA : Zn (w/w%)	Weight of PLGA (g)	Volume of HFIP (mL)	Weight of Zn (g)
PLG-0	14.5	100 : 00	2.71	10	0
PLG-1	14.5	100 : 0.1	1.36	5	0.001
PLG-3	14.5	100 : 0.3	1.36	5	0.004
PLG-5	14.5	100 : 0.5	1.36	5	0.007
PLG-10	14.5	100 : 10	2.71	10	0.271
PLG-30	14.5	100 : 30	2.71	10	0.813
PLG-50	14.5	100 : 50	2.71	10	1.355

Table 2 Composition of PLGA, CH, and Zn in the fabrication of PLC nanofiber meshes

Nanofiber mesh	PLGA : HFIP (w/v%)	PLGA : CH	Proportion of PLGA : Zn (w/w%)	Weight of PLGA (g)	Weight of C (g)	Volume of HFIP (mL)	Weight of Zn (g)
PLC-0	14.5	80 : 20	100 : 00	2.43	0.608	10	0
PLC-1	14.5	80 : 20	100 : 0.1	1.22	0.305	5	0.002
PLC-3	14.5	80 : 20	100 : 0.3	1.22	0.305	5	0.005
PLC-5	14.5	80 : 20	100 : 0.5	1.22	0.305	5	0.008
PLC-10	14.5	80 : 20	100 : 10	2.43	0.608	10	0.243
PLC-30	14.5	80 : 20	100 : 30	2.43	0.608	10	0.729
PLC-50	14.5	80 : 20	100 : 50	2.43	0.608	10	1.215

Fourier-transfer infrared spectroscopy (FTIR) analysis

FTIR was used to identify the functional groups and chemical composition of the nanofiber meshes. An Agilent Cary 630 (Santa Clara, CA, USA) was used to complete the FTIR spectra in the 800–2000 cm^{-1} range. The meshes were studied to understand the modifications sustained by PLG and PLC during electrospinning with Zn nanoparticles.

Differential scanning calorimetry (DSC) analysis and thermogravimetry analysis (TGA)

The temperature and heat flow of the different PLG and PLC nanofiber meshes were evaluated using DSC analysis on a DSC 3+ STARe System (Mettler Toledo, Columbus, OH) over the temperature range of 293–773 K, at a constant rate of 20 K min^{-1}. The first thermal transition peak was used to determine the glass transition temperature (T_g). TGA was used to observe the mass loss and was measured using the TGA/DSC 3+ STARe System (Mettler Toledo, Columbus, OH, USA) in an alumina crucible at room temperature with a temperature range of 293–773 K and a heating rate of 20 K min^{-1}.

Mechanical properties

The mechanical properties of the nanofiber mesh were analyzed using the Instron 3384 (Norwood, MA, USA). A customized template was constructed from cardstock (50 × 35 mm) to hold the mesh in place and ensure uniformity in loading. A nanofiber mesh (40 × 15 mm) was firmly affixed to the template with double-sided tape at both ends before mesh testing. A digital micrometer was used to measure the thickness of the meshes and the average value was used. The affixed nanofiber mesh was placed between the pneumatic jaw gripping, and prior to testing, both sides of the template were cut. Following the literature, the mesh was stretched until failure with a 500 N load cell and a set displacement of 3.5 mm min^{-1}.[22] After each run, a load (N) *versus* extension (mm) curve was generated and the load values were divided by the cross-sectional area (mm^2) to obtain the stress values (MPa). The strain values were calculated by dividing the change in length by the initial length. Stress–strain curves were plotted using Origin Pro, and the Young's modulus (YM) and ultimate tensile strength (UTS) were estimated ($n = 3$).

In vitro degradation and release study of Zn^{2+}

To study the degradation of nanofiber meshes and the release of free Zn^{2+} *in vitro*, PLG and PLC nanofiber meshes (10 × 10 mm) were attached to 24-well plates ($n = 3$) with a surgical silicon adhesive (Kwik-Sil). Nanofiber meshes were sterilized under UV light in a sterile fume hood for approximately 3 h, followed by immersion in 70% ethanol for 30 min and washing twice with DI water. One millimeter of DMEM complete medium, supplemented with 10% fetal bovine serum and 1% antibiotics (10 000 units per mL of penicillin and 10 000 μg per mL of streptomycin) was added to each well containing nanofiber meshes and incubated in a cell culture incubator at 37 °C and 5% CO_2 atmosphere. The medium was collected and replenished at designated time points. Free Zn^{2+} was measured in the diluted collected media using inductively coupled plasma optical emission spectroscopy (ICP-OES Optima 8300, PerkinElmer, Shelton, CT, USA). Before ICP measurements, the collected solutions were diluted. Samples (1 mL) were pipetted into digestion tubes, and concentrated nitric acid (67–70%, Fisher Scientific) and hydrofluoric acid (48–51%, VWR Chemicals) were added to each tube. The digestion tubes underwent a 10-minute predigestion process and were transferred to an automated sequential microwave digester (MARS 6, CEM Microwave Technology Ltd, North Carolina, USA). This resulted in a clear transparent aqueous solution, which was further diluted to 50 mL with double DI water. A set of matrix-matched standards were prepared for the calibration curve. An Optima 8300 ICP-OES instrument was used to analyze the samples. The microwave-assisted digestion of the samples was completed as described in literature.[22]

Cell culture study on nanofibers

Cell preparation. NIH/3T3 fibroblast cell lines derived from mouse embryos (American Type Culture Collection, Manassas, VA, USA) were cultured in complete medium (DMEM with serum and antibiotics, as recommended by ATCC) at 37 °C with 5% CO_2 and 95% humidity. During culture, the medium was replaced every 48 h until the cells reached 90% confluency. Once confluent, cells were passaged by trypsinization before seeding.

Cell seeding to PLGA–Zn and PLGA/CH–Zn nanofiber meshes. Nanofiber meshes from each group ($n = 3$), with the dimensions of 12 × 12 mm were placed into 48-well plates and sterilized under UV light overnight. Next, the meshes were washed with 70% ethanol and phosphate-buffered saline (PBS) (Gibco; Life Technologies). Meshes were pre-treated with DMEM complete medium, supplemented with 10% fetal bovine serum and 1% antibiotics (10 000 units per mL of penicillin and 10 000 μg per mL of streptomycin). Cells with a density of 25 × 10^3 were seeded on each nanofiber mesh by pipetting in the center of the sample and cultured in an incubator for up to 3 days. The medium was replenished every other day. The medium at a volume of 250 μL was collected and stored for toxicity studies.

Cell viability and toxicity analysis. The Alamar Blue (AB) colorimetric assay was used to study the viability of NIH/3T3 cells. Cell-laden nanofiber meshes were treated with 10% AB reagent in the cultured media and incubated for 4 h. Fluorescence was measured at 570 nm excitation and 600 nm emission with a microplate reader (CLARIOstar Plus, BMG LABTECH Inc., Cary, NC, USA), and the assay solutions were transferred to a 96-well plate. Referring to the manufacturer's instructions the cell toxicity of the PLG and PLC nanofiber meshes was assessed using a Pierce LDH assay kit.[38,39] 50 μL of sample medium ($n = 3$), was transferred to a 96-well plate and mixed with 50 μL of the reaction mixture. The plate was covered with aluminium foil and incubated at room temperature for 30 min. The reaction was terminated by adding 50 μL stop solution to each well, and the absorbance of the samples was measured at 490 nm with 680 nm as a reference using a microplate reader.

The proliferation, adhesion, and survivability of the cells in contact with the nanofiber meshes were studied using a live/dead assay kit (PerkinElmer LLC *Via* AOPI Staining Solution; Fisher Scientific, USA), following the manufacturer's protocol. Live cells were stained green, dead cells were stained red, and images were captured with an Olympus IX83 microscope incorporated with Olympus cellSens Dimension software (Olympus Corporation, Shinjuku, Tokyo, Japan). Live and dead cells were counted from the fluorescence images using ImageJ 1.54g (NIH, Bethesda, MD, USA).

Cell attachment and morphology study. Fluorescence microscopy: morphology of viable cells after seeding onto the nanofiber mesh was visualized under a fluorescence microscope for cells cultured on day 3. Cells were seeded at a density of 50×10^3 cells per well. At the end of day 3, the cells were washed twice with PBS before they were fixed with 4% paraformaldehyde (PFA, Thermo Fisher Scientific) and permeabilized in 0.2% Triton (X-100) (Thermo Fisher Scientific) for 2 min at room temperature. After washing with PBS, the cells were blocked with 1% bovine serum albumin (BSA) was used to block the cells for 30 min. Under dark conditions at room temperature, the cytoplasm of the cells attached to the nanofiber mesh was stained with Actin Red 555 Ready probes reagent (Invitrogen, Thermo Fisher Scientific) for 20 min, and the nuclei were stained with DAPI (4′6-diamidino-2-phenylindole dihydrochloride; Invitrogen, Thermo Fisher Scientific) for 5 min. The meshes were washed three times with PBS and fluorescence images were captured using an Olympus IX83 microscope (Olympus).

SEM imaging: following the procedure seen in literature cellular mass attachment, proliferation, and morphology were analyzed using SEM.[37] Attached cells were rinsed twice with PBS and preserved in 4% paraformaldehyde. The cells were rinsed with PBS and dehydrated with successive incubations in 10, 30, 50, 70, and 90% ethanol at room temperature. The meshes were left in a sterile fume hood to dry, and then sputter-coated with palladium gold before images were taken. In addition, the scratch assay was conducted to observe the migration of the cells (SI).

Statistical analysis

The mean and standard deviation (S. D.) were computed for the data for all samples. Data was analyzed by one-way analysis of variance (ANOVA) for significance using the OriginPro software version 2024 (Origin Lab, Northampton, MA, USA). Multiple comparisons were performed using the *post hoc* Tukey's test. Values for alpha were set to 0.05, 0.01, and 0.001, and p values less than 0.05 and 0.001 were considered statistically significant.

Results & discussion

Characterization of nanofiber meshes

Morphology of PLGA–Zn and PLGA/CH–Zn nanofiber. The size and morphology of the as-received Zn nanoparticles used in our nanofiber fabrication, similar to prior work, were a mixture of ultra-small and large aggregated particles as provided by the manufacturer.[22] The fibrous morphology and diameter distribution of the PLG and PLC nanofiber meshes are shown in Fig. 1 and 2, respectively. EDS, a feature of SEM (Hitachi SU8000, Tokyo, Japan), was used to collect elemental data on the PLG and PLC nanofiber meshes (Fig. S1). The fiber morphology varied drastically with changes in the ratios of the polymer and Zn particles. PLG-0 and PLC-0 fibers appear smooth, while PLG and PLC fibers incorporated with Zn present beaded defects on the surface, indicating the effect of Zn particles. As the concentration of Zn increased, aggregated particles were observed on the surface of the fibers. The diameters of the PLG fibers are shown in Fig. 1 and range from 0.14–2.10 μm. The average diameters of PLG-0, PLG-10, PLG-30, and PLG-50 were estimated as 0.60 ± 0.26, 0.43 ± 0.22, 0.71 ± 0.34, and 0.44 ± 0.17 μm respectively. The diameters of the PLC fibers are shown in Fig. 2 and range between 0.08–2.11 μm. The average diameters of PLC-0, PLC-10, PLC-30, and PLC-50 are

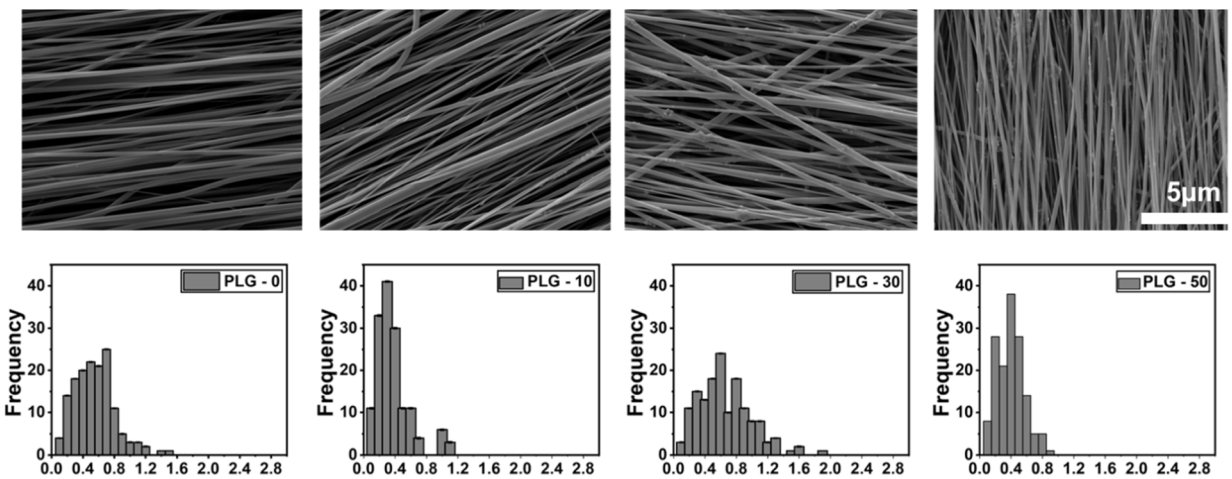

Fig. 1 Surface morphology and diameter distribution of PLG–Zn nanofiber scaffolds. (Left to right) SEM images of PLG-0, PLG-10, LG-30, and PLG-50 scaffolds and corresponding histogram of fiber diameter distribution.

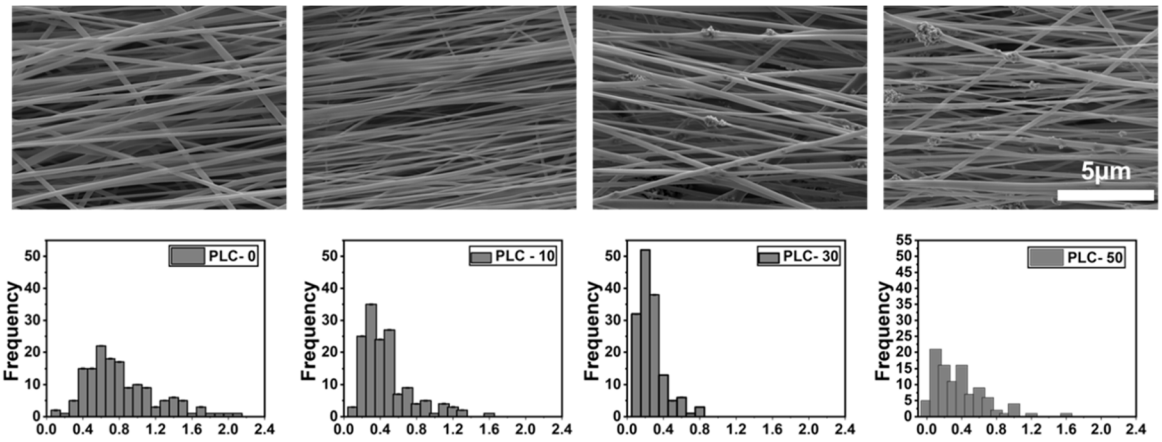

Fig. 2 Surface morphology and diameter distribution of PLC–Zn nanofiber meshes. (Left to right) SEM images of PLC-0, PLC-10, PLC-30, and PLC-50 nanofiber meshes and corresponding histogram of fiber diameter distribution.

estimated as 0.88 ± 0.40, 0.51 ± 0.30, 0.33 ± 0.15, and 0.43 ± 0.29 μm respectively. On average, the diameters of the PLC fibers were smaller than those of the PLG fibers. Similar to the PLG fibers without chitosan, agglomeration occurred with the increased concentration of Zn; however, it appeared that more agglomeration occurred in the PLC fibers than in the PLG fibers because of the inhomogeneous mixing of chitosan with PLGA in the electrospinning solution.

In our observation, there was no significant morphological difference seen between the PLG-0 and PLC-0 and the PLG-1, PLG-3, PLG-5, PLC-1, PLC-3, and PLC-5 nanofiber meshes (results are not included). For the same reason, results are not included in subsequent characterization.

Chemical composition and crystallization properties

The chemical composition of the nanofiber meshes was measured using FTIR to confirm whether the addition of CH and Zn resulted in any chemical changes (Fig. 3). FTIR spectra of PLG meshes were observed at the characteristic peaks of 1751 cm^{-1} (C=O stretch), 864–1452 cm^{-1} (C–H bends), and strong peaks appear between 1085–1182 cm^{-1} (C–O–C stretch).[40] The composite meshes showed a strong peak at 1751 cm^{-1} (C=O stretch) and approximately 2884 cm^{-1} (C–H stretching) and 1626 cm^{-1} (N–H bending). The characteristic peaks of PLG were consistent with previously reported results and showed no significant changes after the incorporation of Zn. The N–H bending peak observed in the PLC nanofiber meshes was indicative of amine groups and confirmed the presence of CH in the mesh. Crystallization properties are shown in SI (Fig. S2). XRD analysis of PLG and PLC nanofiber meshes with varying Zn content revealed distinct peak patterns, indicating the presence of Zn. The results demonstrated the impact of zinc incorporation on the crystalline structure of the nanofiber mesh.

DSC and TGA analysis

PLG–Zn and PLC–Zn thermal behaviours were analyzed using DSC and TGA, to determine if the presence of Zn particles

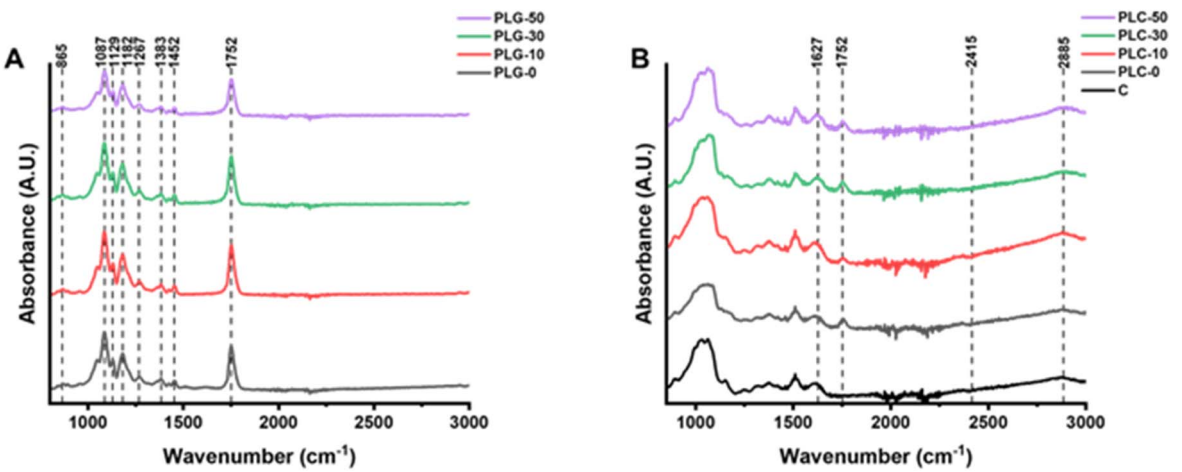

Fig. 3 Chemical composition of the nanofiber meshes. FTIR analysis of chemical compositions of PLG–Zn and PLC–Zn nanofiber meshes (A and B) with different concentrations of Zn NPs. Fig. 4B and C represent the spectra of chitosan.

altered the properties of the nanofiber mesh. When used as wound healing devices, degradation and physical aging are critical for application performance and storage processing. To avoid future problems, such as stability loss or degradation, it is important to understand how a material behaves. Thermal analysis of polymers, such as PLGA, is an appropriate method for providing additional characterization information to aid in application selection, predict product performance, and improve product quality. PLGA is an amorphous material and does not have a melting point. When the temperature of a polymer reaches its glass transition temperature (T_g), the polymer chains begin to move freely, resulting in softening of the material and possible changes in its physical properties.[41–44] DSC was used to study the T_g of the nanofiber meshes. The thermographs in Fig. 4(A and B), show the T_g of each nanofiber mesh. The first endothermic transitions of PLG-0, 10, 30 and 50 were observed at approximately 50.41°, 56.63°, 55.26°, and 51.88° respectively. These transitions correspond to the T_g of PLGA as it is found in literature at approximately 50–58 °C. T_g is a convenient temperature point that indicates the beginning of an evident endothermic reaction.[41,45,46] Thus, the T_g of the nanofiber meshes indicates that they remain stable at room temperature but become flexible at or above physiological temperatures, which is an important property in applications where controlled release and degradation are important, such as drug delivery and biodegradable implants. Additionally, T_g is important when determining a sterilization method for implants because high-heat methods, such as autoclaving, can cause the material to soften, deform, and lose its structural integrity, and devices should be able to maintain their properties until they have concluded their job in their intended application.

TGA determined mass loss due to decomposition.[44] TGA curves Fig. 4(C and D) show the percentage weight loss for the nanofiber meshes. The PLG-0 nanofiber mesh burned completely, whereas the Zn containing meshes retained the metal residue. PLG-0 mesh decomposition started at 300 °C and was completed at 400 °C, matching literature observations of major loss between 290–390 °C.[47] PLG-10, PLG-30, and PLG-50 decomposition began at 220 °C and was completed at 288 °C for PLG-50 and 315 °C for PLG-10 and PLG-30, respectively. While no prior work exists with PLGA and Zn nanoparticles, Khalil *et al.*'s work with silver nanoparticles showed similar trends. Metallic nanoparticles increase thermal conductivity

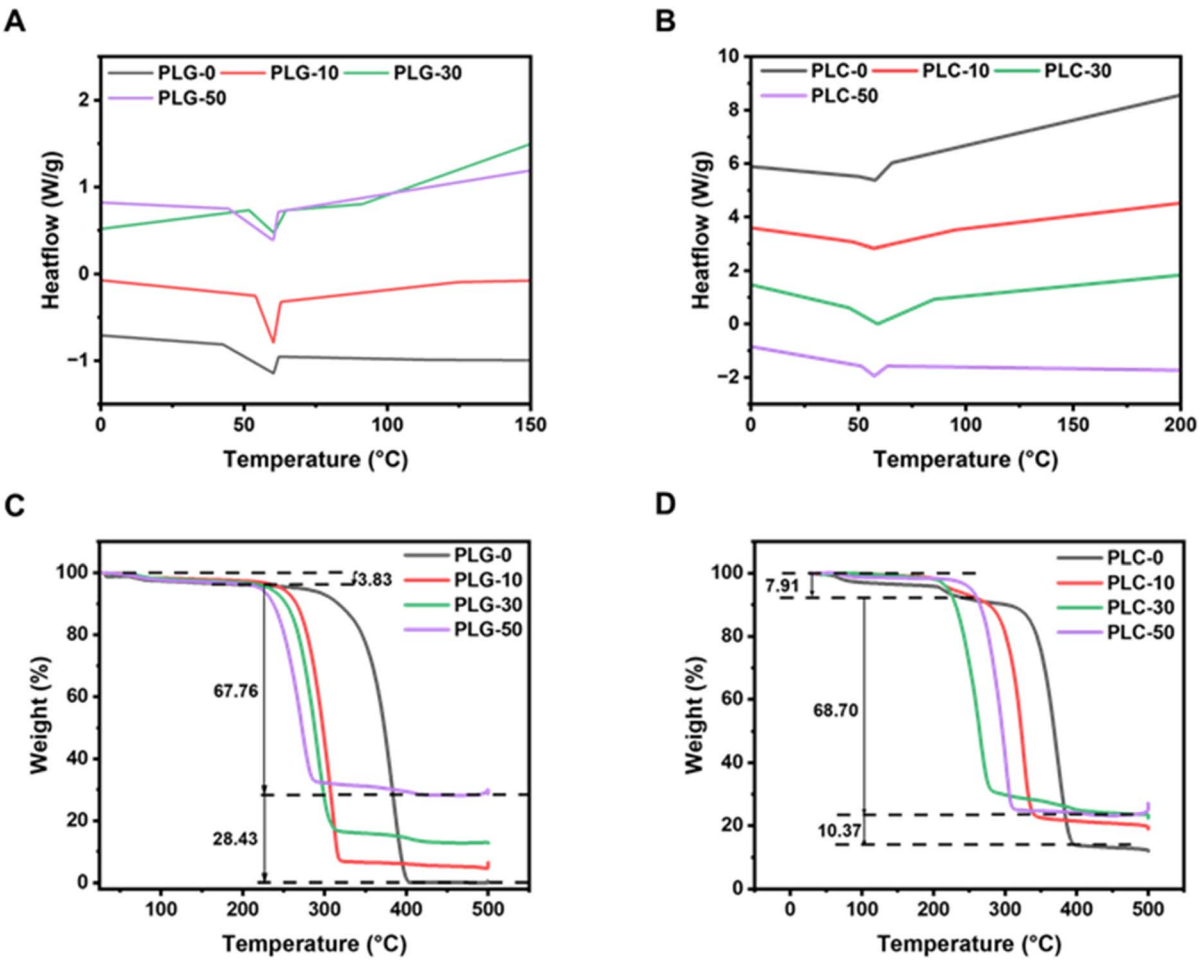

Fig. 4 Thermal analysis of PLG–Zn and PLC–Zn conducted by DSC and TGA respectively. (A and B) DSC curves showing glass transition (T_g) of the respective PLG–Zn and PLC–Zn nanofiber meshes. (C and D) Thermal stability of PLG–Zn and PLC–Zn nanofiber meshes at different temperatures analyzed *via* TGA.

and, affect the decomposition temperature.[48] After decomposition, PLG-10, PLG-30, and PLG-50 retained ~5%, ~13%, and 30% Zn respectively. PLC-0 meshes showed mass changes at 63 °C and 208 °C, with decomposition starting at 320 °C and continuing until 400 °C, retaining trace chitosan. The total weight loss was 88%, which is consistent with the 81–97% range reported in the literature.[49] PLC-10, PLC-30, and PLC-50 decomposed between 205–230 °C and completed between 280–340 °C, with remaining weights of ~5%, ~13%, and ~29%. The decomposition temperature indicates thermal stability under extreme conditions. While nanofiber meshes remain stable under physiological conditions, caution is needed during high-temperature sterilization because of their low T_g. DSC and TGA analyses confirmed the suitability of the material for wound-healing applications based on its thermal properties.

Mechanical properties

It is expected that the combination of particles and polymers of both synthetic and natural origins can significantly alter the mechanical properties of electrospun nanofiber meshes.[37] The stress–strain curves in Fig. 5A and D demonstrate the mechanical properties of the nanofiber meshes. The Young's Modulus (YM), ultimate tensile strength (UTS), and breaking strain quantified from these plots are summarized in Tables S1 and S2. The Young's modulus for PLG-0 was 40.20 ± 6.32 MPa, which is close to the Young's modulus of 37 MPa reported in the literature. The Young's modulus for PLG-10 increased to 48.96 ± 1.63 MPa, while PLG-30 and PLG-50 decreased to 37.41 ± 6.47 MPa and 33.01 ± 3.56 MPa respectively. It is expected that the PLG-10 nanofiber mesh would experience a higher Ultimate Tensile Strength for the PLG–Zn nanofiber meshes, followed by PLG-0 and PLG-30, which were equal. However, the ultimate tensile strength of the PLG-50 meshes decreased. The same trend was also observed in the literature where the incorporation of zinc oxide nanoparticles into polycaprolactone (PCL) or PLGA decreased the tensile strength of the pure matrix. Specifically, Goncharova *et al.* also observed an increase in the strength of their composite materials containing zinc oxide up to 10 wt%, however, materials with higher concentrations demonstrated a decrease in strength.[50] This can be attributed to the intrinsic properties of the composite material; as well as the agglomeration of nanoparticles and high viscosity of the polymer, when mixed this leads to an inhomogeneous dispersion of particles in the polymeric solution.[26,47,50–52] Additionally, the breaking strain for the PLG nanofiber meshes was 1.42 ± 0.16 mm mm^{-1}, 1.39 ± 0.13 mm mm^{-1}, 1.47 ± 0.04 mm mm^{-1} and 1.40 ± 0.14 respectively; suggesting that the nanofiber meshes are able to stretch between 139% to 147% beyond its original length before failure, indicating that the material is highly ductile. As expected, owing to their poor mechanical properties, the inclusion of the natural polymer chitosan into the nanofiber mesh decreased YM, UTS, and BS. The YM for PLC-0 was decreased to 34.65 + 0.83 MPa and PLC-10 was decreased to 34.15 ± 4.41 MPa. The YM of PLC-30 and PLC-50 was decreased to 23.49 ± 2.31 MPa and 12.32 ± 3.48 MPa respectively. The YM of human skin is reported to be between 4.6–20 MPa and the PLC-50 nanofiber meshes fell within this range, whereas the PLC-30 nanofiber meshes YM was decreased very close to the range.[53] Also, in comparison to the PLG–Zn meshes PLC-0 had a higher stress than PLC-10, where PLC-10

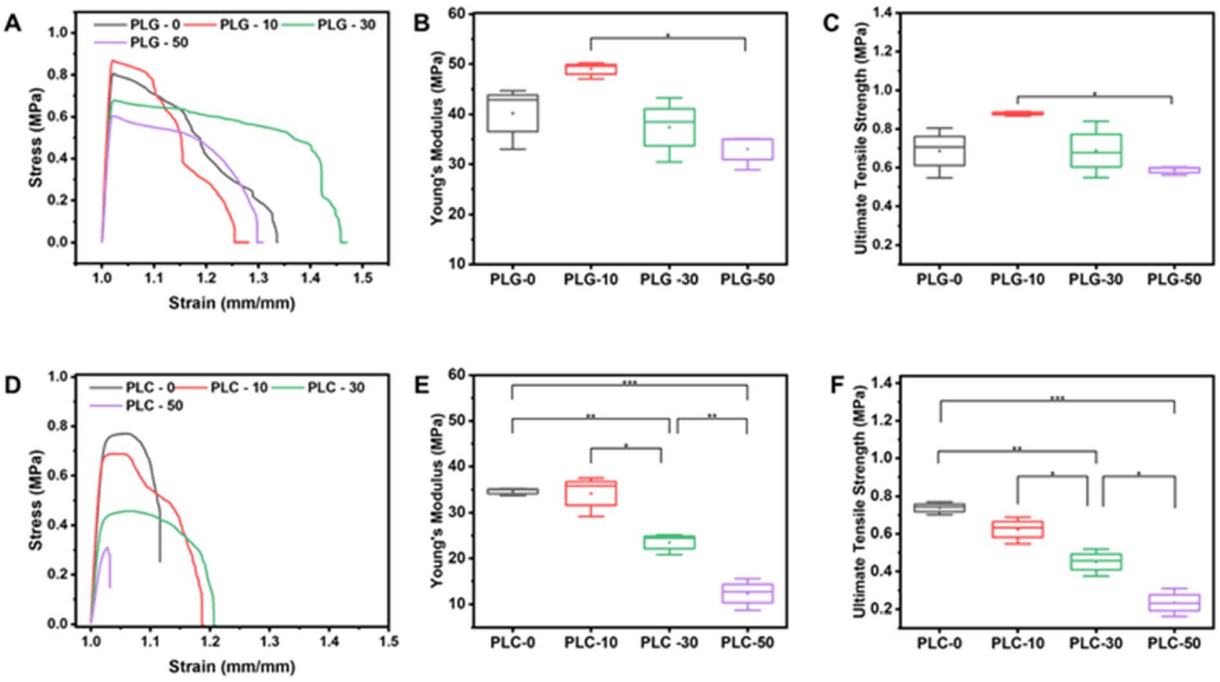

Fig. 5 Analysis of tensile mechanical properties for PLG–Zn and PLC–Zn nanofiber meshes. Representative set of stress–strain curves for PLG–Zn (A) and PLC–Zn (D) nanofiber meshes. Young's modulus comparison for PLG–Zn (B) and PLC–Zn meshes (E). Ultimate tensile strength of PLG–Zn (C) and PLC–Zn (F). Brackets indicate significant differences (ANOVA, *p < 0.05, **p < 0.01, and ***p < 0.1, n = 3).

had a higher stress in comparison to the other Zn-loaded nanofiber meshes. Owing to the poor mechanical properties of chitosan, it is expected that the composite nanofiber meshes containing PLGA and chitosan would show a decrease in mechanical properties, which is evident by the decrease in YM, UTS, and BS for the PLC–Zn nanofiber meshes compared to the PLG–Zn nanofiber mesh. This trend is also evident in other studies containing PLGA and chitosan, where the chitosan-containing nanofibers displayed poorer mechanical properties than pure PLGA nanofibers.[54] The breaking strain for the PLC nanofiber meshes was 1.11 ± 0.01 mm mm^{-1}, 1.17 ± 0.02 mm mm^{-1}, 1.20 ± 0.01 mm mm^{-1}, and 1.04 ± 0.01 mm mm^{-1}, respectively; this suggests that the PLC nanofiber meshes are able to deform between 104% to 120% of its original length before failure. However, in comparison to the PLG nanofiber meshes, this is a decrease in breaking strain, which indicates that the material loses flexibility with the inclusion of chitosan and becomes more brittle.

In vitro release of Zn ions

The release of Zn ions is vital for various cellular functions and tissue healing activities.[22] A Zn ion release study of PLG–Zn and PLC–Zn meshes was conducted in cell culture medium under standard cell culture conditions for mammalian cells for up to 504 h (21 days). The cumulative release of Zn^{2+} was estimated using ICP-OES and microwave-assisted acid digestion was conducted as described in our previous publication.[22] The Zn^{2+} release profiles of the PLG–Zn and PLC–Zn nanofiber meshes are shown in Fig. 6. Fig. 6A and C show the cumulative release of PLG–Zn and PLC–Zn nanofiber meshes, respectively.

Both PLG–Zn and PLC–Zn nanofiber meshes exhibited an increase in Zn^{2+} release as the concentration of the nanofiber meshes increased. Cumulative release of Zn^{2+} was estimated as 0 ± 0, 0.03 ± 0.03, 0.14 ± 0.05, 0.14 ± 0.01 mmol for the PLG-0, PLG-10, PLG-30, and PLG-50 nanofiber meshes respectively at 504 h. PLG–Zn and PLC–Zn nanofiber meshes exhibited an initial burst of release for up to 170 h, followed by a more steady release; however, PLC-10 showed a burst at approximately 336 h (14 days). At the end of the 504 h experiment, the PLC–Zn cumulative release of Zn^{2+} was estimated to be 0 ± 0, 0.046 ± 0.042, 0.215 ± 0.032, and 0.224 ± 0.024 for the PLG-0, PLG-10, PLG-30, and PLG-50, respectively. After 72 h, at 168 h, 336 h, and 504 h, the PLG-0, PLG-10, PLG-30, and PLG-50 values of Zn^{2+} released were all statistically significant ($p < 0.05$). The values for

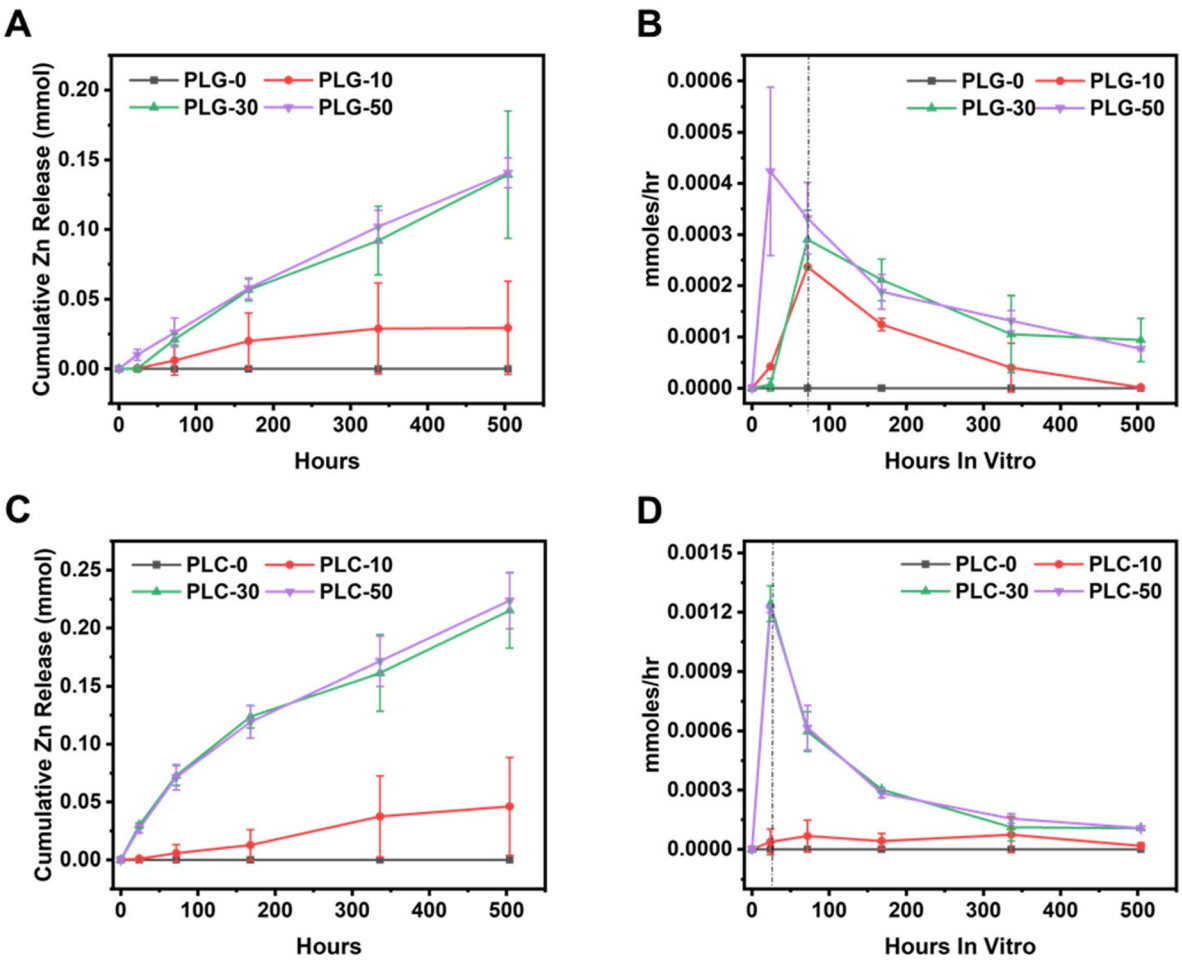

Fig. 6 Study of degradation and release of Zn^{2+} *in vitro*. Cumulative Zn^{2+} release from PLG–Zn (A) and PLC–Zn (C) nanofiber meshes. Hourly Zn release rates for PLG–Zn (B) and PLC–Zn (D) for a 21 day time period. Data are representative of multiple experiments ($n = 3$).

PLC-0, PLC-10, PLC-30, and PLC-50 at the same time points were also statistically significant ($p < 0.05$).

The amount of free Zn^{2+} released was divided by the time of exposure to media (h) to calculate the rate of release for each time period between media replenishment; the rate of release is shown in the graphs in Fig. 6B and D. PLG-10 and PLG-30 scaffolds experienced an increase in release up to 72 h and decreased thereafter; however, PLG-50 experienced an increase in release up to 24 h, followed by a sharp decrease thereafter. PLC-10 nanofiber meshes also experienced an increase in release up to 72 h and a small increase in release at approximately 338 h, however, PLC-30 and PLC-50 experienced an increase in release up to 24 h and a sharp decline at approximately 72 h. Although the rates of release for the nanofiber meshes decreased, the meshes still released Zn at the conclusion of the experiments, except for the PLG-10 and PLC-10 nanofiber meshes, which had nearly released all of the Zn from the nanofiber meshes.

The release experiments were conducted in DMEM supplemented with 10% fetal bovine serum (FBS) to simulate physiological conditions *in vitro*, similar to experiments seen in the literature.[37,55] However, it is important to acknowledge that this medium may result in significant binding of Zn^{2+} by serum proteins, particularly albumin and transferrin, which can reduce the concentration of free Zn^{2+} detectable in the medium. As a result, the measured values may underestimate the total amount of Zn^{2+} released from the nanofiber meshes. Previous experiments comparing ZnO nanoparticle dissolution in DMEM with and without serum have reported lower detected Zn^{2+} concentrations in serum-containing media release, supporting the likelihood of protein binding and chelation in serum-containing media.[56,57] While the current experimental setup

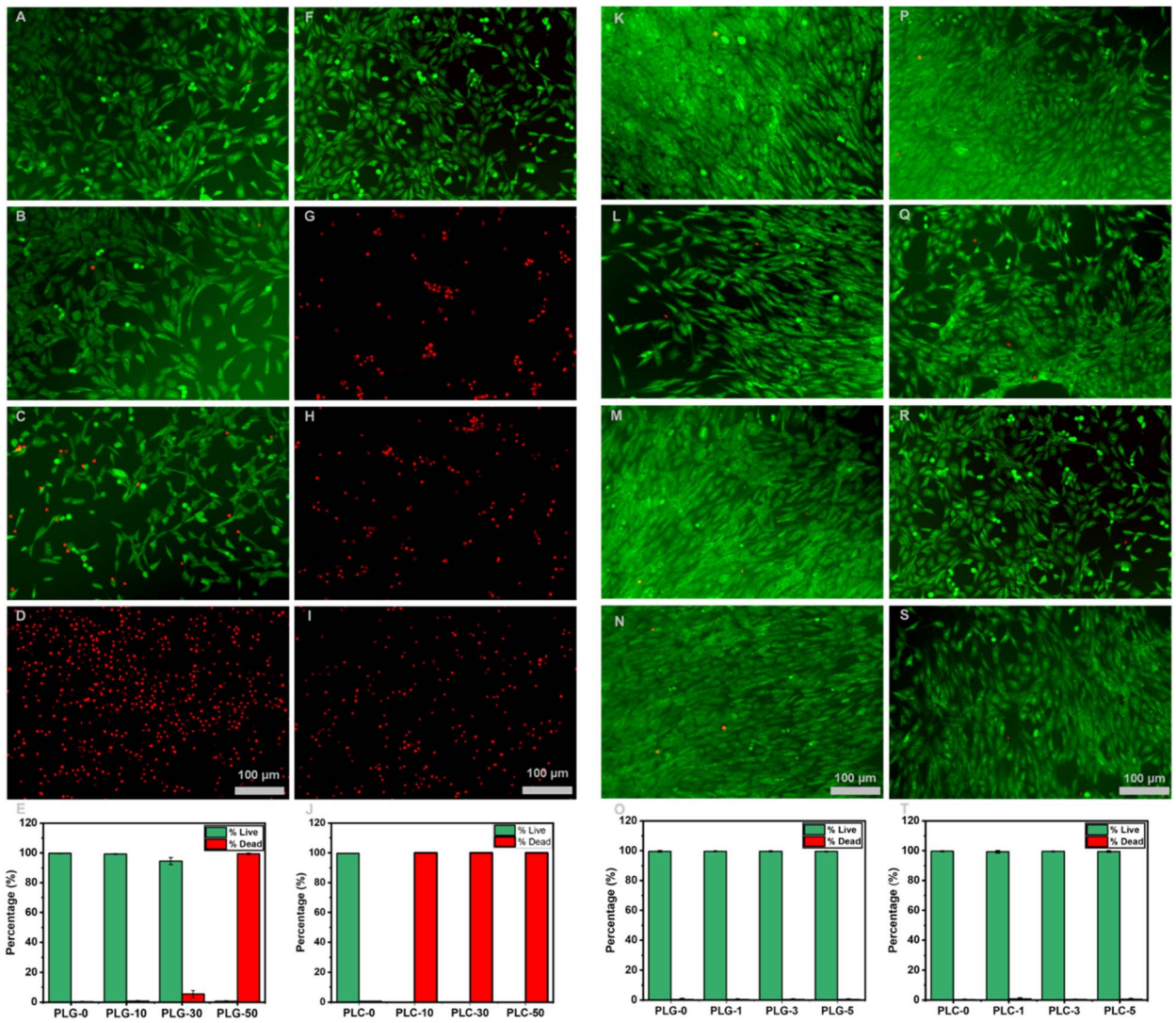

Fig. 7 Live/dead images for PLG-0, PLG-10, PLG-30, and PLG-50 (A–D) and PLC-0, PLC-10, PLC-30, and PLC-50 (F–I) and live and dead cell percentages for PLG–Zn (E) and PLC–Zn (J) for cells cultured on nanofiber meshes. Nanofiber meshes with lower concentrations of Zn are also shown: PLG-0, PLG-1, PLG-3, and PLG-5 (K–N) and PLC-0, PLC-1, PLC-3, and PLC-5 (P–S), and live and dead cell percentages for PLG–Zn (O) and PLC–Zn (T) for cells cultured on nanofiber meshes. A one-way ANOVA test revealed that there were no statistically significant differences in the percentage of live and dead cells across the different Zn-containing nano fiber mesh scaffolds.

reflects biologically relevant conditions, future studies will include PBS-based release assays to quantify the complete release profile in the absence of serum interference.

Electrospun PLGA nanofiber meshes have potential in tissue engineering applications because of their ability to mimic the fibrous ECM of native tissues. Their versatility enables them to be used as temporary ECM for bone, tendon, and nerve regeneration. PLGA nanofiber meshes can be used as a drug delivery system to transport small molecules to large proteins, hydrophilic and hydrophobic and single to multiple molecules. The Zn particles were encapsulated in the polymer matrix. The loaded particles are well protected from degradation and sustainably released from the matrix, reducing the overexposure and over-release of Zn^{2+}. In water, Zn particles are unstable and prone to corrosion, which is further accelerated in electrolyte solutions such as cell culture media. When the PLG and PLC nanofiber meshes were incubated in cell media, they underwent corrosion. Zn particles, incorporated into the fiber matrix and residual on top of the fiber surface, erode when the media permeates through the fiber matrix and Zn ions are released into the media. Also, the degradation behavior of the polymer matrix determines the Zn release profile.[22,49,52,58–60] PLGA is degraded *via* chemical hydrolysis of hydrolytically unstable ester bonds into glycolic and lactic acids. The degradation process of PLGA consists of four steps (i) water penetrates the amorphous region of the polymer and disrupts the secondary forces, (ii) covalent bonds in the backbone of the polymer begins by hydrolysis, during which carboxylic end – groups autocatalyse the hydrolysis reaction, (iii) massive cleavage of the backbone covalent bonds causes significant mass loss, and (iv) the polymer loses weight. Molecular weight, co-polymer ratio, specimen size, environmental conditions, and polydispersity are all factors that influence the degradation behaviour of PLGA. PLGA is generally considered a hydrophobic material; it exhibits hydrophilicity to absorb water and it is degraded by cleavage of hydrolytically sensitive ester bonds. Additionally, blending other additives such as hydrophilic chitosan polymers also influence how quickly the nanofiber meshes degrade; blending PLGA and chitosan facilitated water penetration through composite membranes, and the increasing hydrophilicity affects how quickly the nanofiber meshes degrade.[22,61] PLGA–Zn nanofiber meshes were generally hydrophobic; however, integration of chitosan into the nanofiber meshes increased the degree of hydrophilicity, refer to SI (Fig. S3 and Table S5) for more detailed information about the wettability of the nanofiber meshes.

In vitro cytotoxicity

In addition to *in vitro* cytotoxicity testing, we also observed the antibacterial properties of the nanofiber mesh scaffolds; this information can be found in the SI (Tables S3 and S4).

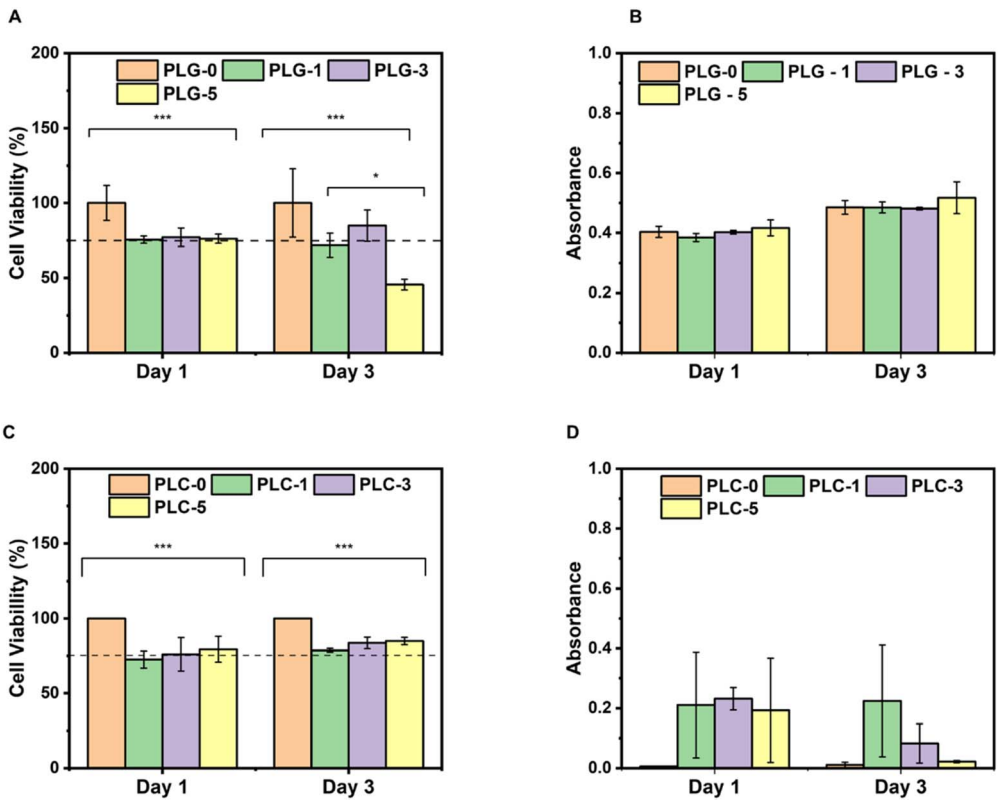

Fig. 8 *In vitro* performance of nanofiber mesh and effects on viability and toxicity of 3T3 fibroblast cells using direct test method. (A and B) Viability (Alamar Blue Assay) and toxicity (LDH absorbance assay) of the cultured cells on the PLG-0, PLG-1, PLG-3, and PLG-5 meshes. (C and D) Viability (Alamar Blue Assay) and toxicity (LDH absorbance assay) of the cultured cells on the PLC-0, PLC-1, PLC-3, and PLC-5 meshes with an 90 : 10 PLGA to chitosan ratio.

According to Tao *et al.*, and confirmed by our studies, Zn^{2+} is toxic at high concentrations.[61] For *in vitro* studies, the solutions were optimized to decrease the chance of Zn^{2+} toxicity.[62,63] Fig. 7 shows live/dead images for PLG-0, PLG-10, PLG-30, PLG-50 (Fig. 7(A–D)), PLC-0, PLC-10, PLC-30, and PLC-50 (Fig. 7(F–I)), and the percentage of live and dead cells within 24 h of culture with the respective nanofiber meshes. Both PLG-50 and PLC-50 showed that 100% of the cells died, suggesting that 50% of Zn was toxic to the cells. PLG-10 and PLG-30 have 99.26 ± 0.304% and 94.56 ± 2.38% respectively. Fig. 7(E and K) show the percentage of live and dead cells for each respective nanofiber mesh. However, the decrease in the percentage of live cells suggests that they were starting to die off. 100% of the PLC-10, PLC-30, and PLC-50 cells were dead. According to literature, the concentration range of Zn^{2+} that promotes cell migration and proliferation are at or below the micromolar range, specifically concentrations less than 100 μM (favorably around 50 μM or lower) have shown to be non-cytotoxic.[64–66] Since Zn^{2+} is toxic at high concentrations, PLG-1, PLG-3, PLG-5, PLC-1, PLC-3, and PLC-5 indicated formulations with decreased Zn concentrations for cell culture studies.[62]

Initial trial experiments with PLGA showed that the 80 : 20 ratio was optimal for this solution. However, after additional trial experiments in SI (Fig. S4), we observed that when mixed with Zn, chitosan used in higher concentrations produced a cytotoxic effect. Chitosan is a positively charged molecule that interacts strongly with negatively charged cell membranes. The presence of chitosan in the fibres generally improves cell adhesion. However, when used as a drug carrier and loaded with a drug, the number of positively charged amino groups that remain available decreases. The consequence of this lower number of charges is a diminished capacity to interact with the cell membrane and surrounding environment, decreasing its uptake and leading to potential toxicity. Several of the previous experiments confirmed that a low concentration of chitosan is sufficient to enhance the biocompatibility of electrospun

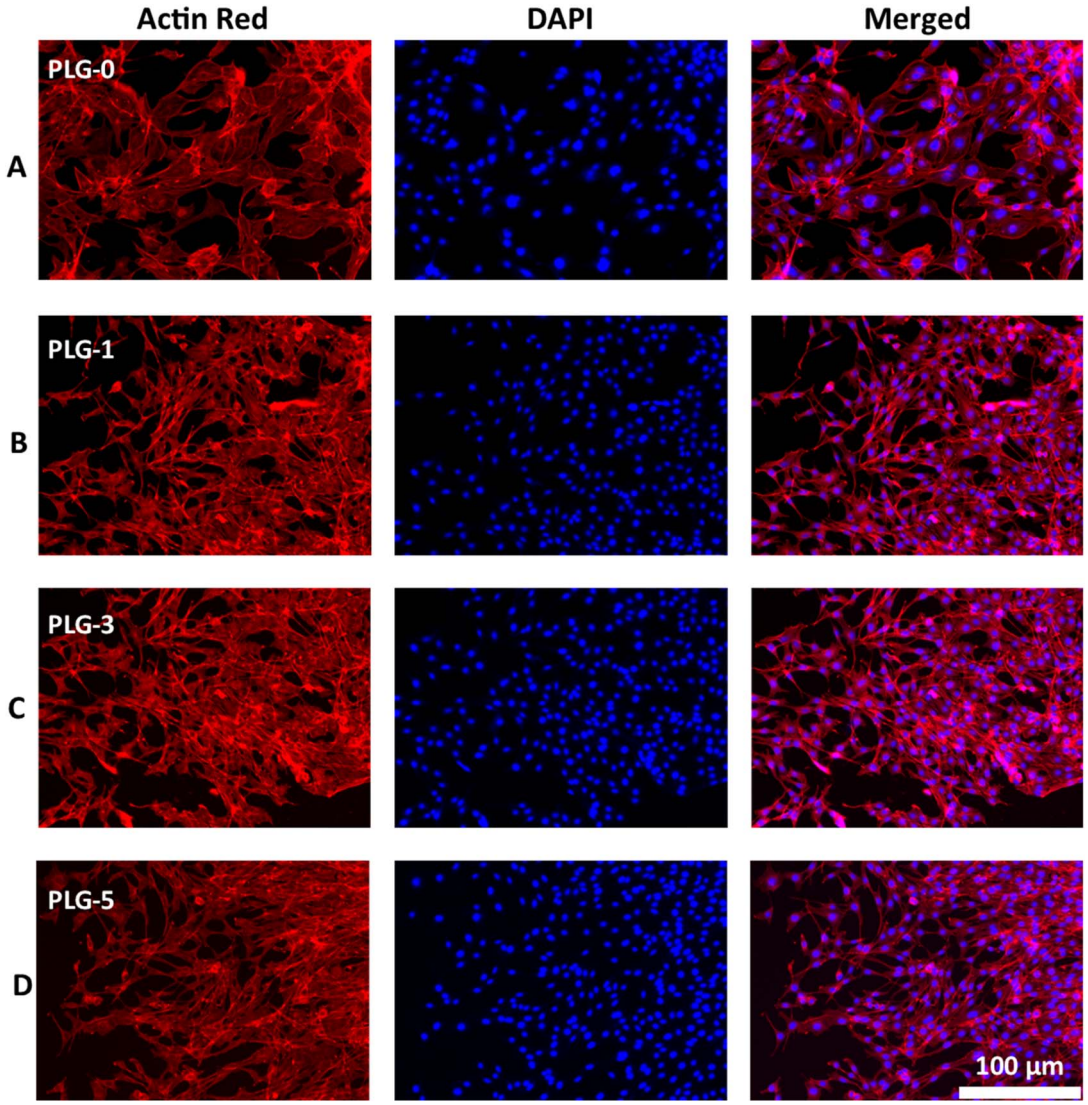

Fig. 9 *In vitro* performance of PLG–Zn (A–D) nanofiber meshes and their effect on cell morphology. Day 3 fluorescence imaging of NIH/3T3 cells cultured on nanofiber meshes. The cytoskeleton was stained with ActinrRed (red) and the nuclei was stained with DAPI (blue).

nanofiber meshess.[67–71] Thus, we decreased the composition to a 90% PLGA and 10% chitosan ratio, without compromising the concentration of Zn, in the meshes to optimize the performance *in vitro*. All data referenced from here on out has been obtained using the 90 : 10 PLGA : chitosan nanofiber meshes. Fig. 7(K–N and P–S) shows the cell attachment and proliferation of the NIH/3T3 fibroblast cells when cultured with the PLG-0, PLG-1, PLG-3, and PLG-5 (Fig. 7(K–N)) and PLC-0, PLC-1, PLC-3, and PLC-5 (Fig. 7(P–S)). Fig. 7(O and T) shows the percentage of live and dead cells for each respective nanofiber mesh. Green indicates that cells are alive and red indicates that cells are dead. The live/dead images further show how the cells are beginning to migrate. Additionally, all nanofiber meshes have ~99% of live cells on day 3.

Alamar Blue and LDH assays were used to study the cell viability and cytotoxicity of the PLG–Zn and PLC–Zn nanofiber meshes. The cells were seeded directly onto the nanofiber meshes and examined for 1, 3, and 6 days. PLG-0 and PLC-0 nanofiber meshes were used as the positive controls. The ISO 10993-5 standard for cell viability states that cell viability higher than 75% is considered non-toxic for medical devices; thus, nanofiber meshes containing Zn that expressed viability at or above this standard were considered safe.[72]

Fig. 8A, shows that all nanofiber meshes containing Zn were viable on day 1, with PLG-1 having 76%, PLG-3 77%, and PLG-5 76%. On day 3, of the Zn-containing meshes, only the PLG-3 meshes met the minimum standard for viability at 85%. PLG-1 and PLG-5 showed cell viabilities of 72% and 45%, respectively. Based on ICP data, it appears that day 3 (72 h) is the time point when the nanofiber meshes released the most Zn, which could possibly explain why some nanofiber meshes were not viable on day 3. Additionally, it is possible that the lack of cell-

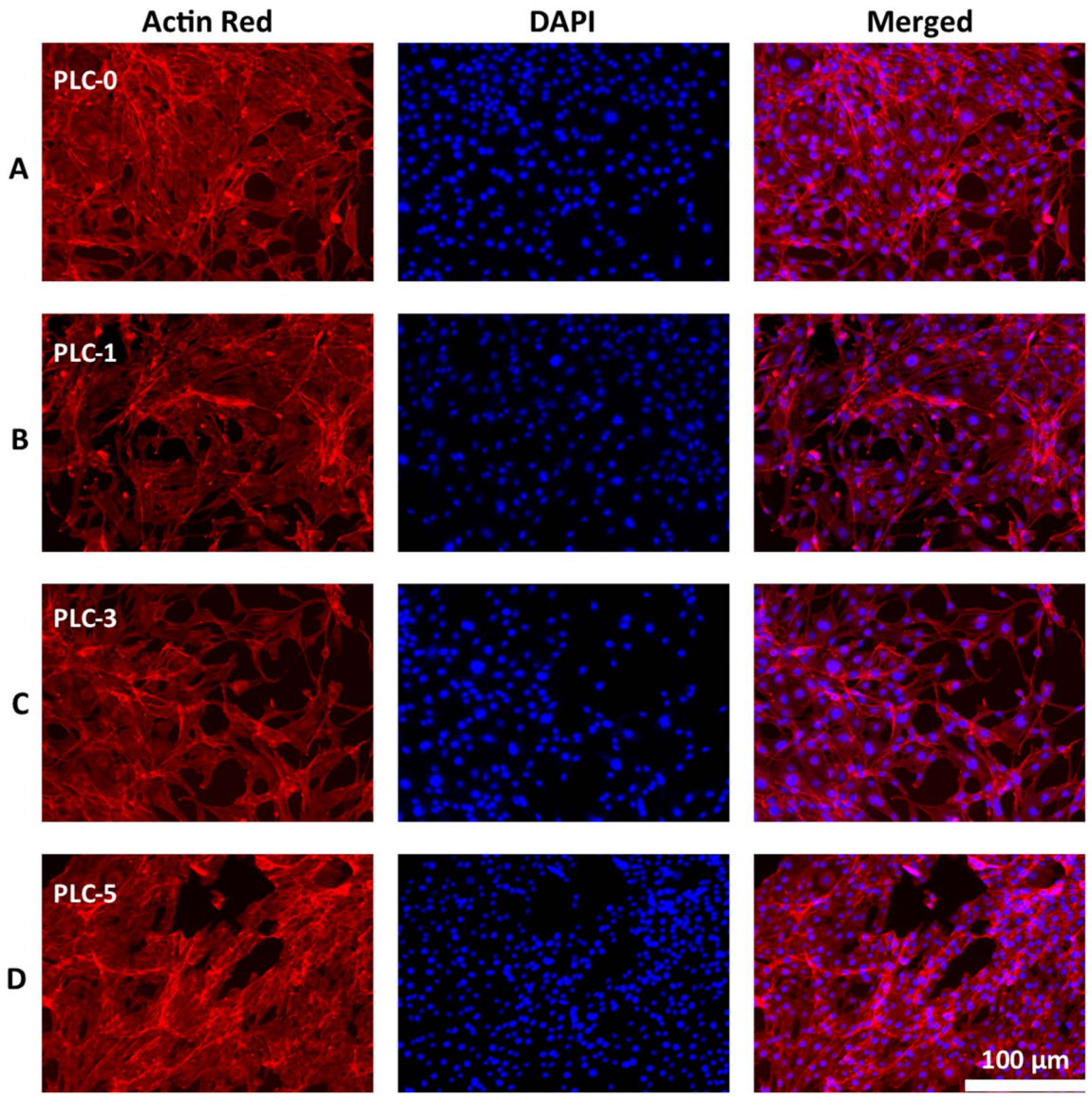

Fig. 10 *In vitro* performance of PLC–Zn (A–D) nanofiber meshes and their effect on cell morphology. Day 3 fluorescence imaging of NIH/3T3 cells cultured on nanofiber meshes. The cytoskeleton was stained with ActinRed (red) and the nuclei was stained with DAPI (blue).

recognition sites in the synthetic polymer and the release of solvent traces during the first couple of days could also contribute to poor cell viability on day 3.[68]

Cell viability for the 90 : 10 PLGA : chitosan nanofiber meshes is shown in Fig. 8C and D and are referenced as PLC-0, PLC-1, PLC-3, and PLC-5. On day 1, PLC-3 and PLC-5 nanofiber meshes were both at 75% and 79% viability, respectively. PLC-1 was slightly below the minimum threshold for viability at 72%. On day 3, all nanofiber meshes were above the threshold at 79%, 83%, and 85% for PLC-1, PLC-3, and PLC-5, respectively. Since by day 3, PLC-1 was above the minimum threshold of viability. However, the cell viability of PLC-1 was observed slightly lower but was almost similar to other groups, indicating there was no significant difference compared to among.

The enzyme lactate dehydrogenase (LDH) delivery assay was used to assess cytotoxicity. LDH is an intracellular enzyme and its increased presence in the cellular environment suggests problems with the cytoplasmic membrane, leading to cell damage. LDH assay measures cellular membrane permeabilization (rupture) and severe irreversible cell damage.[73] The higher the LDH concentration, the higher the cell death rate.[74] LDH activity is dependent on cell number, suggesting that higher cell concentrations are more cytotoxic.[75] Fig. 8B shows the optical density (OD) for the LDH assay for PLG–Zn meshes. The cytotoxicity on all experimental days was relatively low, indicating that the meshes initially had low toxicity. However, the cytotoxicity increased slightly over the 3-day experiment. The cytotoxicity of PLC–Zn meshes, Fig. 8D, remained relatively low; however, the cytotoxicity of these meshes was more variable. A limitation of this study is the reliance on viability-based toxicity assays, which, while informative for preliminary screening, do not capture the full spectrum of cellular responses. Future investigations should incorporate additional toxicity biomarkers, including oxidative stress parameters, to better elucidate the underlying mechanisms of action.

The fluorescence images in Fig. 9 and 10 show the morphology of the NIH/3T3 fibroblast cells after cell seeding on

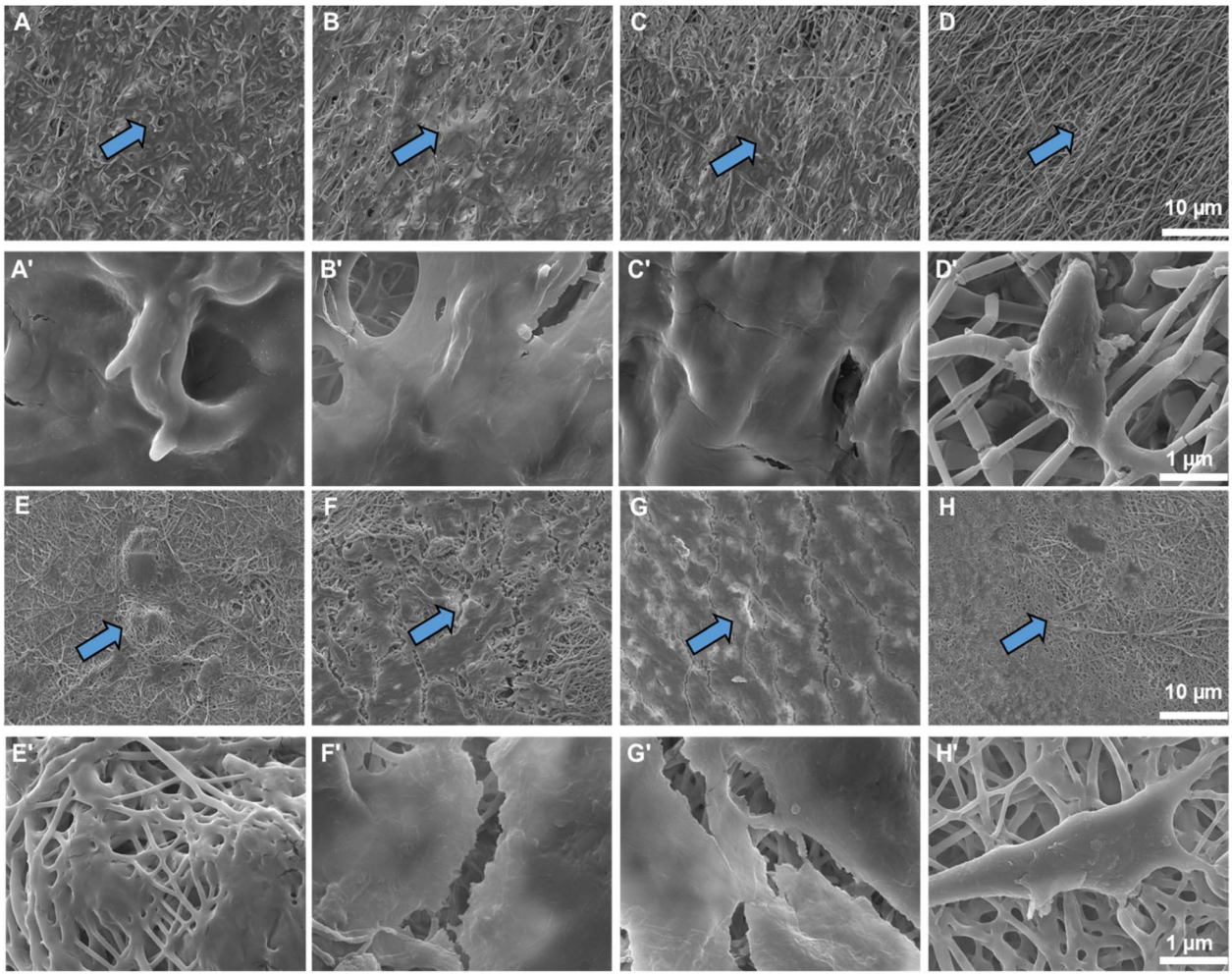

Fig. 11 SEM images of *in vitro* performance of nanofiber meshes and effects on cell morphology and attachment. NIH/3T3 fibroblast were cultured for 3 days on PLG-0, PLG-1, PLG-3, and PLG-5 (A–D) respectively. High resolution images (A′–D′) are shown corresponding to their respective images in (A–D). SEM images of *in vitro* performance of nanofiber meshes and effects on cell morphology and attachment. NIH/3T3 fibroblast were cultured for 3 days on PLC-0, PLC-1, PLC-3, and PLC-5 (E–H) respectively. High resolution images (E′–H′) are shown corresponding to their respective images in (E–H).

nanofiber meshes on day 3. ActinRed was used to stain the cytoskeleton and DAPI was used to stain the nuclei. Both the cytoskeleton and nuclei were intact for all PLG–Zn and PLC–Zn nanofiber meshes. Images were taken at the edge of the nanofiber meshes, instead of the center, which has a higher cell density owing to issues with obtaining clear, flat images. Nonetheless, images show cellular attachment, migration, and proliferation on day 3 when cells are exposed to Zn^{2+} released into the cell media.

The SEM data further evaluated the cellular compatibility of the PLG–Zn and PLC–Zn nanofiber meshes. SEM images revealed the attachment of cells seeded directly onto the nanofiber mesh. Fig. 11 shows the SEM images of NIH/3T3 fibroblast cells taken after culturing with the PLG-0, PLG-1, PLG-3, and PLG-5 (Fig. 11A–D and A′–D′′) nanofiber meshes, respectively. The SEM images showed that PLG-0, PLG-1, and PLG-3 exhibited better attachment and migration with the fibers. As expected, PLG-5 performed worse because of the higher concentration of Zn. Fig. 11 also shows the SEM images of NIH/3T3 fibroblast cells taken after culturing with the PLC-0, PLC-1, PLC-3, and PLC-5 (Fig. 11E–H and E′–H′′) nanofiber meshes. The cells were well attached to the PLC–Zn meshes, and the addition of chitosan appeared to have had a better effect on cell migration. PLC-1, and especially PLC-3, indicate that the cells have almost completely migrated together, which suggests favorable activity for wound healing. While PLC-5 showed good migration, it was not as strong as PLC-3, which again is indicative of the higher concentration of Zn exhibiting some form of toxicity to the cells.

***In vitro* scratch assay.** A wound healing scratch assay is used to study the rate of closure of a scratch *in vitro*. This test allows for the study of cell migration in a controlled manner.[53] Fig. S5 shows the scratch assay for PLG-0, PLG-1, PLG-3, and PLG-5 nanofiber meshes, respectively. Fig. S7A, reports the percentage of wound closure as approximately 86%, 73%, 76%, and 41% for the PLG-0, PLG-1, PLG-3, and PLG-5 nanofiber meshes respectively. These results are consistent with our cell viability studies in that after 24 h all wounds begin to close at a slower rate when compared to the PLG-0 control. Nonetheless, PLG-1 and PLG-3 both showed a steady closure rate between 73% and 76% which suggests that increasing the Zn concentration increased the closure rate. However, it is interesting to note that the closure rate of PLG-5 at 41% was unexpectedly low, which can be attributed to the lack of cell recognition sites in the synthetic polymer. Alternatively, scratch assay results for PLC-0, PLC-1, PLC-3, and PLC-5 are shown in Fig. S6 and the percentage of wound closure is reported in Fig. S7B as 69%, 32%, 52%, and 89%, respectively. This also suggests that the increasing Zn concentration increased the closure rate, and is consistent with results seen in the literature, where the inclusion of chitosan in the composite material showed favorable healing abilities.[75]

Conclusions

This study aimed to synthesize a Zn-integrated PLGA/chitosan nanofiber mesh for potential wound-healing applications. Using the electrospinning technique, we fabricated biodegradable PLGA–Zn (*i.e.* PLG–Zn) and PLGA/CH–Zn (*i.e.* PLC–Zn) composite nanofiber meshes with different concentrations of Zn particles. The physical, chemical, and biological properties of the composite nanofiber meshes were analyzed. The fiber morphology, thermal stability, mechanical properties, and biological properties were very dependent composition of chitosan and Zn. The incorporation of Zn into the meshes and the synthesis of the composite meshes drastically changed the fiber morphology. The incorporation of Zn did not change the chemical composition of the PLG or the PLC meshes. Integrating Zn into the PLG and PLC meshes did not significantly alter the melting and crystallization temperatures, however, the endothermic reaction for the composite materials of PLC was more spontaneous. As expected, complete weight loss was observed for the PLG and PLC meshes that did not contain Zn. However, the weight loss of the Zn-containing meshes was consistent with the amounts of Zn present in the respective meshes. Compared to the meshes without Zn, the PLG-10 and PLC-10 meshes exhibited higher strengths. Zn ion release studies have shown that nanofiber meshes with higher Zn concentrations release more Zn^{2+}. This is consistent with expectations, as there was more Zn to be released from these meshes. *In vitro* studies showed that PLG–Zn and PLC–Zn nanofiber meshes with high Zn concentrations (*e.g.*, more than 10%) are toxic, causing complete cell death. Lower Zn concentrations (1%, 3%, 5%) significantly improve biocompatibility, with PLG-3 and PLC-3 and PLC-5 showing the best performance in terms of cell viability (>75% on day 3), low cytotoxicity, and enhanced cell attachment, migration, and proliferation. The inclusion of chitosan in the nanofiber meshes increased the hydrophilicity of the composite material. Future work would need to be completed to determine how the concentration would directly affect other properties. The inclusion of chitosan in the PLGA fibrous mesh at low concentration enhances the bioactivity and minimizes Zn^{2+} toxicity, suggesting that these meshes may be suitable for applications like wound healing and tissue engineering. However, while the *in vitro* findings demonstrate encouraging biocompatibility, further validation through *in vivo* wound healing studies is necessary to assess performance under physiological conditions and to substantiate their clinical potential.

Author contributions

Conceptualization, N. B.; methodology, D. D. and S.S., investigation, D. D., A. M., S. S., R. A., and K. S.; formal analysis, N. B., J. S. and D. D.; writing – original draft, D. D; writing – reviewing & editing, A. M., J. S., and N. B., project administration, N. B.

Conflicts of interest

There are no conflicts to declare.

Data availability

All data generated in this study will be made available by the corresponding author on reasonable request.

Supplementary information: surface morphology analysis by SEM-EDS; X-ray diffraction analysis; antimicrobial properties; water contact angle measurement, *in vitro* cytotoxicity; and scratch assay. See DOI: **https://doi.org/10.1039/d5ra03639a**.

Acknowledgements

This work was supported financially by the National Science Foundation-Excellence in Research (NSF-EiR 2100861). Part of this research work was supported by NSF Engineering Research Centre for Hybrid Autonomous Manufacturing Moving from Evolution to Revolution (ERC-HAMMER) (EEC-2133630), and Chancellor's Distinguished Fellowship (Title III HBGI grant from the U.S. Department of Education). We thank Dr Svitlana and Dr Boyce Collins for their technical assistance in research. Characterization of the scaffolds was also performed in part at the Joint School of Nanoscience and Nanoengineering (SENIC-NNCI), which is supported by the National Science Foundation (NSF ECCS-1542174) and facilities of the College of Engineering. Illustration for Table of Contents was created with **https://www.biorender.com/**. The authors acknowledge the Analytical Services Laboratory at the College of Agriculture and Environmental Sciences, North Carolina A&T State University, for their valuable support in facilitating the sample preparation and elemental analysis.

Notes and references

1 Y. Dong, Y. Zheng, K. Zhang, Y. Yao, L. Wang, X. Li, J. Yu and B. Ding, Electrospun Nanofibrous Materials for Wound Healing, *Adv. Fiber Mater.*, 2020, **2**, 212–227, DOI: **10.1007/s42765-020-00034-y**.

2 C. He, B. Yu, Y. Lv, Y. Huang, J. Guo, L. Li, M. Chen, Y. Zheng, M. Liu, S. Guo, X. Shi and J. Yang, Biomimetic Asymmetric Composite Dressing by Electrospinning with Aligned Nanofibrous and Micropatterned Structures for Severe Burn Wound Healing, *ACS Appl. Mater. Interfaces*, 2022, **14**, 32799–32812, DOI: **10.1021/acsami.2c04323**.

3 R. Dong, Y. Li, M. Chen, P. Xiao, Y. Wu, K. Zhou, Z. Zhao and B. Z. Tang, In Situ Electrospinning of Aggregation-Induced Emission Nanofibrous Dressing for Wound Healing, *Small Methods*, 2022, **6**, 2101247, DOI: **10.1002/smtd.202101247**.

4 H. Park, T. V. Patil, S. D. Dutta, J. Lee, K. Ganguly, A. Randhawa, H. Kim and K. Lim, Extracellular Matrix-Bioinspired Anisotropic Topographical Cues of Electrospun Nanofibers: A Strategy of Wound Healing through Macrophage Polarization, *Adv. Healthcare Mater.*, 2024, **13**, 2304114, DOI: **10.1002/adhm.202304114**.

5 Y. Peng, Y. Ma, Y. Bao, Z. Liu, L. Chen, F. Dai and Z. Li, Electrospun PLGA/SF/artemisinin composite nanofibrous membranes for wound dressing, *Int. J. Biol. Macromol.*, 2021, **183**, 68–78, DOI: **10.1016/j.ijbiomac.2021.04.021**.

6 M. Z. Zulkifli, D. Nordin, N. Shaari and S. K. Kamarudin, Overview of Electrospinning for Tissue Engineering Applications, *Polymers*, 2023, **15**, 2418, DOI: **10.3390/polym15112418**.

7 L. Sethuram and J. Thomas, Therapeutic applications of electrospun nanofibers impregnated with various biological macromolecules for effective wound healing strategy – A review, *Biomed. Pharmacother.*, 2023, **157**, 113996, DOI: **10.1016/j.biopha.2022.113996**.

8 X. Zhang, Y. Wang, Z. Gao, X. Mao, J. Cheng, L. Huang and J. Tang, Advances in wound dressing based on electrospinning nanofibers, *J. Appl. Polym. Sci.*, 2024, **141**, e54746, DOI: **10.1002/app.54746**.

9 C. Lee, S. Huang, K. Hung, C. Cho and S. Liu, Enhanced Diabetic Wound Healing Using Electrospun Biocompatible PLGA-Based Saxagliptin Fibrous Membranes, *Nanomaterials*, 2022, **12**, 740, DOI: **10.3390/nano12213740**.

10 M. Gaur, S. Maurya, M. S. Akhtar and A. B. Yadav, Synthesis and Evaluation of BSA-Loaded PLGA–Chitosan Composite Nanoparticles for the Protein-Based Drug Delivery System, *ACS Omega*, 2023, **8**, 18751–18759, DOI: **10.1021/acsomega.3c00738**.

11 A. M. Maadani, F. Davoodian and E. Salahinejad, Effects of PLGA coating on biological and mechanical behaviors of tissue engineering scaffolds, *Prog. Org. Coat.*, 2023, **176**, 107406, DOI: **10.1016/j.porgcoat.2023.107406**.

12 G. Ajmal, G. V. Bonde, P. Mittal, V. K. Pandey, N. Yadav and B. Mishra, PLGA/Gelatin-based electrospun nanofiber scaffold encapsulating antibacterial and antioxidant molecules for accelerated tissue regeneration, *Mater. Today Commun.*, 2023, **35**, 105633, DOI: **10.1016/j.mtcomm.2023.105633**.

13 H. M. Azzazy, S. A. Fahmy, N. K. Mahdy, M. R. Meselhy and U. Bakowsky, Chitosan-Coated PLGA Nanoparticles Loaded with Peganum harmala Alkaloids with Promising Antibacterial and Wound Healing Activities, *Nanomaterials*, 2021, **11**, 2438, DOI: **10.3390/nano11092438**.

14 Y. Wang, L. Guo, J. Liu, X. Huang, X. Wang, X. Guo, X. You, W. Li, L. Li, T. Sun and Y. Gao, Chitosan/PLGA shell nanoparticles as Tylotoin delivery platform for advanced wound healing, *Int. J. Biol. Macromol.*, 2022, **220**, 395–405, DOI: **10.1016/j.ijbiomac.2022.07.244**.

15 R. A. Jain, The manufacturing techniques of various drug loaded biodegradable poly(lactide-co-glycolide) (PLGA) devices, *Biomaterials*, 2000, **21**, 2475–2490, DOI: **10.1016/S0142-9612(00)00115-0**.

16 Y. A. Amnieh, S. Ghadirian, N. Mohammadi, M. Shadkhast and S. Karbasi, Evaluation of the effects of chitosan nanoparticles on polyhydroxy butyrate electrospun scaffolds for cartilage tissue engineering applications, *Int. J. Biol. Macromol.*, 2023, **249**, 126064, DOI: **10.1016/j.ijbiomac.2023.126064**.

17 C. Cui, S. Sun, S. Wu, S. Chen, J. Ma and F. Zhou, Electrospun chitosan nanofibers for wound healing application, *Eng. Regener.*, 2021, **2**, 82–90, DOI: **10.1016/j.engreg.2021.08.001**.

18 H. Liu, C. Wang, C. Li, Y. Qin, Z. Wang, F. Yang, Z. Li and J. Wang, A functional chitosan-based hydrogel as a wound dressing and drug delivery system in the treatment of wound healing, *RSC Adv.*, 2018, **8**, 7533–7549, DOI: **10.1039/C7RA13510F**.

19 J. Shah, D. Patel, D. Rananavare, D. Hudson, M. Tran, R. Schloss, N. Langrana, F. Berthiaume and S. Kumar, Recent Advancements in Chitosan-Based Biomaterials for Wound Healing, *J. Funct. Biomater.*, 2025, **16**, 45, DOI: 10.3390/jfb16020045.

20 P. Feng, Y. Luo, C. Ke, H. Qiu, W. Wang, Y. Zhu, R. Hou, L. Xu and S. Wu, Chitosan-Based Functional Materials for Skin Wound Repair: Mechanisms and Applications, *Front. Bioeng. Biotechnol.*, 2021, **9**, 650598.

21 J. J. D. Venezuela, S. Johnston and M. S. Dargusch, The Prospects for Biodegradable Zinc in Wound Closure Applications, *Adv. Healthcare Mater.*, 2019, **8**, 1900408, DOI: 10.1002/adhm.201900408.

22 F. Tettey, S. Saudi, D. Davies, S. Shrestha, K. Johnson, S. Fialkova, K. Subedi, B. P. Bastakoti, J. Sankar, S. Desai and N. Bhattarai, Fabrication and Characterization of Zn Particle Incorporated Fibrous Scaffolds for Potential Application in Tissue Healing and Regeneration, *ACS Appl. Mater. Interfaces*, 2023, **15**, 48913–48929, DOI: 10.1021/acsami.3c09793.

23 G. Katarivas Levy, J. Goldman and E. Aghion, The Prospects of Zinc as a Structural Material for Biodegradable Implants—A Review Paper, *Metals*, 2017, **7**, 402, DOI: 10.3390/met7100402.

24 N. Yang, J. Venezuela, S. Almathami and M. Dargusch, Zinc-nutrient element based alloys for absorbable wound closure devices fabrication: Current status, challenges, and future prospects, *Biomaterials*, 2022, **280**, 121301, DOI: 10.1016/j.biomaterials.2021.121301.

25 P. Lin, M. Sermersheim, H. Li, P. H. U. Lee, S. M. Steinberg and J. Ma, Zinc in Wound Healing Modulation, *Nutrients*, 2018, **10**, 16, DOI: 10.3390/nu10010016.

26 D. A. Canales, N. Piñones, M. Saavedra, C. Loyo, H. Palza, L. Peponi, A. Leonés, R. V. Baier, A. R. Boccaccini, A. Grünelwald and P. A. Zapata, Fabrication and assessment of bifunctional electrospun poly(l-lactic acid) scaffolds with bioglass and zinc oxide nanoparticles for bone tissue engineering, *Int. J. Biol. Macromol.*, 2023, **228**, 78–88, DOI: 10.1016/j.ijbiomac.2022.12.195.

27 D. Banerjee, S. Vishwakarma, M. Nayak, A. Upadhyay, L. Pradhan, P. Makam and S. Mukherjee, Fabrication of Zinc-Tryptophan Nanoassemblies for Antibacterial and Wound Healing Applications, *ACS Appl. Nano Mater.*, 2025, **8**, 4263–4278, DOI: 10.1021/acsanm.5c00657.

28 Y. Chen, J. Cai, D. Liu, S. Liu, D. Lei, L. Zheng, Q. Wei and M. Gao, Zinc-based metal organic framework with antibacterial and anti-inflammatory properties for promoting wound healing, *Regener. Biomater.*, 2022, **9**, rbac019, DOI: 10.1093/rb/rbac019.

29 F. Zhou, S. Sun, C. Cui, X. Li, S. Wu, J. Ma, S. Chen and C. M. Li, Zinc ions and ciprofloxacin-encapsulated chitosan/poly(ε-caprolactone) composite nanofibers promote wound healing via enhanced antibacterial and immunomodulatory, *Int. J. Biol. Macromol.*, 2023, **253**, 127086, DOI: 10.1016/j.ijbiomac.2023.127086.

30 S. Che, Y. Yang, Z. Li, Z. Su and S. Zhang, Integration of Zn2+, ATP, and bFGF to Nanodressing with Core–Shell Structure Fabricated by Emulsion Electrospinning for Wound Healing, *ACS Appl. Bio Mater.*, 2024, **7**, 3316–3329, DOI: 10.1021/acsabm.4c00258.

31 S. Gunturu and T. S. Dharmarajan, in *Copper and Zinc*, ed. Pitchumoni, C. S. and Dharmarajan, T. S., Geriatric Gastroenterology, Springer International Publishing, Cham, 2020, pp 1–17.

32 H. Schoofs, J. Schmit and L. Rink, Zinc Toxicity: Understanding the Limits, *Molecules*, 2024, **29**, 3130, DOI: 10.3390/molecules29133130.

33 N. Molaee, S. Fahimirad, A. Ganji and H. Abtahi, Carboxymethyl bacterial cellulose electrospun nanofibers loaded with zinc oxide nanoparticles and polyhexamethylene biguanide for wound healing promotion, *J. Biomater. Sci., Polym. Ed.*, 2025, 1–36, DOI: 10.1080/09205063.2025.2490079.

34 M. Kuddushi, T. Kumar, H. Wu, S. Chen, B. Bin Xu, N. Malek, L. Unsworth, J. Xu, J. Zhang, X. Wang and X. Zhang, A semi-transparent strong biomimetic wound healing material: zinc oxide and sodium alginate based bi-layer nanofiber membrane, *Adv. Compos. Hybrid Mater.*, 2025, **8**, 179, DOI: 10.1007/s42114-025-01269-2.

35 M. M. Nemati, R. Heidari, A. Keshavarzi, A. Ahmadi, M. Abedi, S. Ranjbar and Y. Ghasemi, In Vitro and In Vivo Evaluation of Electrospun PVA Nanofiber Containing ZnO/Curcumin for Wound Healing Application, *Appl. Biochem. Biotechnol.*, 2025, **197**, 194–215, DOI: 10.1007/s12010-024-05018-x.

36 F. Zhou, C. Cui, S. Sun, S. Wu, S. Chen, J. Ma and C. M. Li, Electrospun ZnO-loaded chitosan/PCL bilayer membranes with spatially designed structure for accelerated wound healing, *Carbohydr. Polym.*, 2022, **282**, 119131, DOI: 10.1016/j.carbpol.2022.119131.

37 U. Adhikari, X. An, N. Rijal, T. Hopkins, S. Khanal, T. Chavez, R. Tatu, J. Sankar, K. J. Little, D. B. Hom, N. Bhattarai and S. K. Pixley, Embedding magnesium metallic particles in polycaprolactone nanofiber mesh improves applicability for biomedical applications, *Acta Biomater.*, 2019, **98**, 215–234, DOI: 10.1016/j.actbio.2019.04.061.

38 B. P. Bastakoti, N. Bhattarai, M. D. Ashie, F. Tettey, S. Yusa and K. Nakashima, Single-Micelle-Templated Synthesis of Hollow Barium Carbonate Nanoparticle for Drug Delivery, *Polymers*, 2023, **15**, DOI: 10.3390/polym15071739.

39 S. Tatum, F. Tettey-Engmann, R. Bhandari, N. Bhattarai and S. Saudi, A Novel Hydrogel-Bronchial Epithelial Cell Spheroids For Toxicological Evaluation, *Biomed. Sci. Instrum.*, 2021, **57**, 406–419, DOI: 10.34107/KSZV7781.10406.

40 G. Singh, K. Tanurajvir, K. Ravinder and A. Kaur, Recent biomedical applications and patents on biodegradable polymer-PLGA, *Int. J. Pharmacol. Pharm. Sci.*, 2014, **1**, 30–42.

41 N. Zhang, C. Wang, H. Chen, J. Wu, C. C. Han and S. Xu, Electrospun Fibrous Membrane with Confined Chain Configuration: Dynamic Relaxation and Glass Transition, *Polymers*, 2022, **14**(5), 939, DOI: 10.3390/polym14050939.

42 N. Na, M. Kim, J. Kim and J. Chang, Fabrication and Customization of Highly Porous PLGA Membranes Utilizing Near-Field Electrospinning, Thermal Transitions,

and Multilayer Strategies, *Adv. Eng. Mater.*, 2024, **26**, 2400917, DOI: 10.1002/adem.202400917.

43 F. N. Almajhdi, H. Fouad, K. A. Khalil, H. M. Awad, S. H. S. Mohamed, T. Elsarnagawy, A. M. Albarrag, F. Al-Jassir and H. S. Abdo, In-vitro anticancer and antimicrobial activities of PLGA/silver nanofiber composites prepared by electrospinning, *J. Mater. Sci.:Mater. Med.*, 2014, **25**, 1045–1053, DOI: 10.1007/s10856-013-5131-y.

44 M. F. Silva, A. A. W. Hechenleitner, J. M. Irache, A. J. A. d. Oliveira and E. A. G. Pineda, Study of thermal degradation of PLGA, PLGA nanospheres and PLGA/maghemite superparamagnetic nanospheres, *Mater. Res.*, 2015, **18**, 1400–1406.

45 G. G. Rivelli, A. C. Perez, P. H. R. Silva, E. C. d. L. Gomes, C. P. d. S. Moreira, E. Tamashiro, F. C. P. Valera, W. T. Anselmo-Lima, G. A. Pianetti and A. Silva-Cunha, Biodegradable Electrospun Nanofibers: A New Approach For Rhinosinusitis Treatment, *Eur. J. Pharm. Sci.*, 2021, **163**, 105852, DOI: 10.1016/j.ejps.2021.105852.

46 N. Alnuman, R. Al-Jafary, F. Manna and R. Almuhtaseb, Fabrication and Characterization of Electrospun 75:25 PLGA Nanofibers for Skin Tissue Engineering, *2018 IEEE-EMBS Conference on Biomedical Engineering and Sciences (IECBES)*, 2018, pp. 560–565.

47 J. A. Abdullah, J. J. Benítez, A. Guerrero and A. Romero, Sustainable Integration of Zinc Oxide Nanoparticles: Enhancing Properties of Poly(ε-Caprolactone) Electrospun Nanofibers and Cast Films, *Coatings*, 2023, **13**(10), 1665, DOI: 10.3390/coatings13101665.

48 K. A. Khalil, H. Fouad, T. Elsarnagawy and F. N. Almajhdi, Preparation and Characterization of Electrospun PLGA/silver Composite Nanofibers for Biomedical Applications, *Int. J. Electrochem. Sci.*, 2013, **8**, 3483–3493, DOI: 10.1016/S1452-3981(23)14406-3.

49 B. Wang, G. Lu, K. Song, A. Chen, H. Xing, J. Wu, Q. Sun, G. Li and M. Cai, PLGA-based electrospun nanofibers loaded with dual bioactive agent loaded scaffold as a potential wound dressing material, *Colloids Surf., B*, 2023, **231**, 113570, DOI: 10.1016/j.colsurfb.2023.113570.

50 D. A. Goncharova, E. N. Bolbasov, A. L. Nemoykina, A. A. Aljulaih, T. S. Tverdokhlebova, S. A. Kulinich and V. A. Svetlichnyi, Structure and Properties of Biodegradable PLLA/ZnO Composite Membrane Produced via Electrospinning, *Materials*, 2021, **14**(1), 2, DOI: 10.3390/ma14010002.

51 B. Wang, G. Lu, K. Song, A. Chen, H. Xing, J. Wu, Q. Sun, G. Li and M. Cai, PLGA-based electrospun nanofibers loaded with dual bioactive agent loaded scaffold as a potential wound dressing material, *Colloids Surf., B*, 2023, **231**, 113570, DOI: 10.1016/j.colsurfb.2023.113570.

52 D. Hajzamani, P. Shokrollahi, N. Najmoddin and F. Shokrolahi, Effect of engineered PLGA-gelatin-chitosan/PLGA-gelatin/PLGA-gelatin-graphene three-layer scaffold on adhesion/proliferation of HUVECs, *Polym. Adv. Technol.*, 2020, **31**, 1896–1910, DOI: 10.1002/pat.4915.

53 A. Moody and N. Bhattarai, Enhanced Cell Proliferation, Migration, and Fibroblast Differentiation with Electrospun PCL–Zinc Scaffolds Coated with Fibroblast-Derived ECM, *ACS Omega*, 2025, **10**, 4427–4441.

54 A. D. Li, Z. Z. Sun, M. Zhou, X. X. Xu, J. Y. Ma, W. Zheng, H. M. Zhou, L. Li and Y. F. Zheng, Electrospun Chitosan-graft-PLGA nanofibres with significantly enhanced hydrophilicity and improved mechanical property, *Colloids Surf., B*, 2013, **102**, 674–681, DOI: 10.1016/j.colsurfb.2012.09.035.

55 S. Shrestha, B. K. Shrestha, F. Tettey-Engmann, R. B. Z. Auniq, K. Subedi, S. Ghimire, S. Desai and N. Bhattarai, Zein-Coated Zn Metal Particles-Incorporated Nanofibers: A Potent Fibrous Platform for Loading and Release of Zn Ions for Wound Healing Application, *ACS Appl. Mater. Interfaces*, 2024, **16**, 49197–49217, DOI: 10.1021/acsami.4c13458.

56 C. M. S. Michielsen, E. A. van Aalen and M. Merkx, Ratiometric Bioluminescent Zinc Sensor Proteins to Quantify Serum and Intracellular Free Zn2+, *ACS Chem. Biol.*, 2022, **17**, 1567–1576, DOI: 10.1021/acschembio.2c00227.

57 I. Hsiao and Y. Huang, Effects of serum on cytotoxicity of nano- and micro-sized ZnO particles, *J. Nanopart. Res.*, 2013, **15**, 1829, DOI: 10.1007/s11051-013-1829-5.

58 M. El Khatib, V. Russo, G. Prencipe, A. Mauro, R. Wyrwa, G. Grimm, M. Di Mattia, P. Berardinelli, M. Schnabelrauch and B. Barboni, Amniotic Epithelial Stem Cells Counteract Acidic Degradation By-Products of Electrospun PLGA Scaffold by Improving Their Immunomodulatory Profile In Vitro, *Cells*, 2021, **10**(11), 3221, DOI: 10.3390/cells10113221.

59 B. Wang, G. Lu, K. Song, A. Chen, H. Xing, J. Wu, Q. Sun, G. Li and M. Cai, PLGA-based electrospun nanofibers loaded with dual bioactive agent loaded scaffold as a potential wound dressing material, *Colloids Surf., B*, 2023, **231**, 113570, DOI: 10.1016/j.colsurfb.2023.113570.

60 B. Duan, L. Wu, X. Li, X. Yuan, X. Li, Y. Zhang and K. Yao, Degradation of electrospun PLGA-chitosan/PVA membranes and their cytocompatibility in vitro, *J. Biomater. Sci., Polym. Ed.*, 2007, **18**, 95–115, DOI: 10.1163/156856207779146105.

61 B. Tao, C. Lin, X. Qin, Y. Yu, A. Guo, K. Li, H. Tian, W. Yi, D. Lei, Y. Chen and L. Chen, Fabrication of gelatin-based and Zn2+-incorporated composite hydrogel for accelerated infected wound healing, *Mater. Today Bio*, 2022, **13**, 100216, DOI: 10.1016/j.mtbio.2022.100216.

62 B. Ekram, M. A. E.-H. Bothaina, M. E.-K. Abeer, T. F. Mohamed, I. S. Zeinab, M. A. Sherif, H. Gabr, I. W. Ahmed and W. G. Osiris, Enhanced mesenchymal stem cells growth on antibacterial microgrooved electrospun zinc chloride/polycaprolactone conduits for peripheral nerve regeneration, *J. Bioact. Compat. Polym.*, 2021, **36**, 152–168, DOI: 10.1177/0883911520988305.

63 I. Sahibdad, S. Khalid, G. R. Chaudhry, A. Salim, S. Begum and I. Khan, Zinc enhances the cell adhesion, migration, and self-renewal potential of human umbilical cord

derived mesenchymal stem cells, *World J. Stem Cell.*, 2023, **15**, 751–767, DOI: 10.4252/wjsc.v15.i7.751.

64 B. Salesa and R. Sabater I Serra, Serrano-Aroca, Á Zinc Chloride: Time-Dependent Cytotoxicity, Proliferation and Promotion of Glycoprotein Synthesis and Antioxidant Gene Expression in Human Keratinocytes, *Biology*, 2021, **10**, 1072, DOI: 10.3390/biology10111072.

65 M. Olea-Flores, J. Kan, A. Carlson, S. A. Syed, C. McCann, V. Mondal, C. Szady, H. M. Ricker, A. McQueen, J. G. Navea, L. A. Caromile and T. Padilla-Benavides, ZIP11 Regulates Nuclear Zinc Homeostasis in HeLa Cells and Is Required for Proliferation and Establishment of the Carcinogenic Phenotype, *Front. Cell Dev. Biol.*, 2022, **10**, 895433, DOI: 10.3389/fcell.2022.895433.

66 T. Fukunishi, C. A. Best, T. Sugiura, T. Shoji, T. Yi, B. Udelsman, D. Ohst, C. S. Ong, H. Zhang, T. Shinoka, C. K. Breuer, J. Johnson and N. Hibino, Tissue-Engineered Small Diameter Arterial Vascular Grafts from Cell-Free Nanofiber PCL/Chitosan Scaffolds in a Sheep Model, *PLoS One*, 2016, **11**, e0158555.

67 E. Bolaina-Lorenzo, C. Martínez-Ramos, M. Monleón-Pradas, W. Herrera-Kao, J. V. Cauich-Rodríguez and J. Cervantes-Uc, Electrospun polycaprolactone/chitosan scaffolds for nerve tissue engineering: physicochemical characterization and Schwann cell biocompatibility, *Biomed. Mater.*, 2016, **12**, 015008, DOI: 10.1088/1748-605X/12/1/015008.

68 Q. Li, E. T. Dunn, E. W. Grandmaison and M. F. A. Goosen, Applications and Properties of Chitosan, *J. Bioact. Compat. Polym.*, 1992, **7**, 370–397, DOI: 10.1177/088391159200700406.

69 E. Khor and L. Y. Lim, Implantable applications of chitin and chitosan, *Biomaterials*, 2003, **24**, 2339–2349, DOI: 10.1016/s0142-9612(03)00026-7.

70 S. Rodrigues, M. Dionísio, C. R. López and A. Grenha, Biocompatibility of Chitosan Carriers with Application in Drug Delivery, *J. Funct. Biomater.*, 2012, **3**, 641, DOI: 10.3390/jfb3030615.

71 J. Wang, F. Witte, T. Xi, Y. Zheng, K. Yang, Y. Yang, D. Zhao, J. Meng, Y. Li, W. Li, K. Chan and L. Qin, Recommendation for modifying current cytotoxicity testing standards for biodegradable magnesium-based materials, *Acta Biomater.*, 2015, **21**, 237–249, DOI: 10.1016/j.actbio.2015.04.011.

72 C. B. Weldon, J. H. Tsui, S. A. Shankarappa, V. T. Nguyen, M. Ma, D. G. Anderson and D. S. Kohane, Electrospun drug-eluting sutures for local anesthesia, *J. Controlled Release*, 2012, **161**, 903–909, DOI: 10.1016/j.jconrel.2012.05.021.

73 G. Zanatta, M. Rudisile, M. Camassola, J. Wendorff, N. Nardi, C. Gottfried, P. Pranke and C. A. Netto, Mesenchymal stem cell adherence on poly(D, L-lactide-Co-glycolide) nanofibers scaffold is integrin-β1 receptor dependent, *J. Biomed. Nanotechnol.*, 2012, **8**, 211–218, DOI: 10.1166/jbn.2012.1382.

74 M. Khandaker, N. Alkadhem, H. Progri, S. Nikfarjam, J. Jeon, H. Kotturi and M. B. Vaughan, Glutathione Immobilized Polycaprolactone Nanofiber Mesh as a Dermal Drug Delivery Mechanism for Wound Healing in a Diabetic Patient, *Processes*, 2022, **10**(3), 512, DOI: 10.3390/pr10030512.

75 H. Adeli, M. T. Khorasani and M. Parvazinia, Wound dressing based on electrospun PVA/chitosan/starch nanofibrous mats: Fabrication, antibacterial and cytocompatibility evaluation and in vitro healing assay, *Int. J. Biol. Macromol.*, 2019, **122**, 238–254.